Modulating glial genes involved in synaptic function mitigates pathogenesis and behavioral deficits in a *Drosophila* model of Huntington's Disease

Tarik S. Onur[1,2,3,+], Andrew Laitman[2,4,5,+], He Zhao[2], Ryan Keyho[2], Hyemin Kim[2], Jennifer Wang[2], Megan Mair[1,2,3], Alma Perez[2], Maria de Haro[1,2], Huilan Wang[6], Ying-Wooi Wan[2], Genevera Allen[2,7], Boxun Lu[6], Ismael Al-Ramahi[1,2], Zhandong Liu[2,4,5], Juan Botas[1,2,3,4,8*]

[1] Department of Molecular and Human Genetics, Baylor College of Medicine, Houston, Texas, USA
[2] Jan and Dan Duncan Neurological Research Institute at Texas Children's Hospital, Houston, Texas, USA
[3] Genetics & Genomics Graduate Program, Baylor College of Medicine, Houston, Texas, USA
[4] Quantitative & Computational Biosciences, Baylor College of Medicine, Houston, Texas, USA
[5] Department of Pediatrics, Baylor College of Medicine, Houston, Texas, USA
[6] State Key Laboratory of Medical Neurobiology and MOE Frontiers Center for Brain Science, School of Life Sciences, Fudan University, Shanghai, China
[7] Departments of Electrical and Computer Engineering, Statistics and Computer Science, Rice University, Houston, Texas, USA
[8] Lead Contact
* Correspondence: jbotas@bcm.edu
[+] Co-first authors

Abstract

Most research on neurodegenerative diseases has focused on neurons, yet glia help form and maintain the synapses whose loss is so prominent in these conditions. To investigate the contributions of glia to Huntington's disease (HD), we studied transcriptomic changes in HD human, HD mice, and *Drosophila* expressing human mutant *Huntingtin* (m*HTT*) in either glia, neurons or both. A large portion of conserved genes are concordantly dysregulated across the three species; we tested these genes in a high-throughput behavioral assay and found that downregulation of genes involved in synapse assembly mitigated pathogenesis and behavioral deficits. To our surprise, mitigating glial pathogenesis by d*NRXN3* knockdown was sufficient to improve the phenotype of flies expressing m*HTT* in neurons, suggesting that mHTT's toxic effects in glia ramify throughout the brain. This supports a model in which dampening synaptic function is protective because it attenuates the excitotoxicity that characterizes HD.

Introduction

Neurodegenerative conditions involve a complex cascade of events that takes many years to unfold. Even in the case of inherited disorders due to mutation in a single gene, such as Huntington's Disease (HD), the downstream ramifications at the molecular level are astonishingly broad. Caused by a CAG repeat expansion in *Huntingtin* (*HTT*) (The Huntington's Disease Collaborative Research Group, 1993), HD pathology is prominent in the striatum and cortex, yet transcriptomic studies consistently reveal thousands of changes in gene expression across the brain and different neuronal cell types, involving pathways ranging from autophagy to vesicular trafficking (Saudou and Humbert, 2016). To disentangle changes that are pathogenic from those that represent the brain's effort to compensate for the disease, we recently integrated transcriptomics with *in silico* analysis and high-throughput *in vivo* screening using a *Drosophila* model of HD (Al-Ramahi et al., 2018). This study demonstrated that HD pathogenesis is driven by upregulation of genes involved in the actin cytoskeleton and inflammation, but that neurons compensate by downregulating the expression of genes involved in synaptic biology and calcium signaling.

The finding that synaptic changes were protective caught our attention, because HTT itself is necessary for normal synaptogenesis and maintenance within the cortico-striatal circuit (McKinstry et al., 2014), largely through its role in retrograde axonal trafficking of neurotrophic factors (Saudou and Humbert, 2016). But synapses involve more than just neurons: glial cells also contribute to synapse formation, function, and elimination (Filipello et al., 2018; McKinstry et al., 2014; Octeau et al., 2018; Stogsdill et al., 2017). There is, in fact, emerging evidence that various glial subtypes affect outcomes in HD. The accumulation of mHTT in astrocytes and oligodendrocytes hinders their development and function and contributes to disease pathophysiology (Benraiss et al., 2016; Ferrari Bardile et al., 2019; Osipovitch et al., 2019; Wood et al., 2018). Conversely, healthy glia can improve the disease phenotype in HD mice (Benraiss et al., 2016). Recent studies using single-cell sequencing in astrocytes isolated from post-mortem tissue from HD patients and mouse models of HD (Al-Dalahmah et al., 2020; Diaz-Castro et al., 2019) developed molecular profiles that distinguish HD-affected astrocytes from astrocytes found in healthy brain tissue, but the physiological consequences of the gene expression changes were unclear. Whether mHTT affects glial participation in synapse formation or maintenance remains unknown, but then, we are only just now beginning to understand the range of glial types and their functions (Bayraktar et al., 2020; Darmanis et al., 2015).

The combination of synaptic degeneration in HD and the fact that both HTT and glia contribute to synaptic formation and maintenance led us to further investigate the influence of *mHTT* in glia. Because *Drosophila* have been used to elucidate glial biology (Freeman and Doherty, 2006; Olsen and Feany, 2019; Pearce et al., 2015; Ziegenfuss et al., 2012) and are a tractable model system for studying HD and

other neurodegenerative diseases (Al-Ramahi et al., 2018; Bondar et al., 2018; Donnelly et al., 2020; Fernandez-Funez et al., 2000; Filimonenko et al., 2010; Goodman et al., 2019; Ochaba et al., 2014; Olsen and Feany, 2019; O'Rourke et al., 2013; Rousseaux et al., 2018; Yuva-Aydemir et al., 2018), we decided to generate flies that express m*HTT* solely in glia so that we could compare their transcriptomic signature with that of flies expressing m*HTT* in neurons. We took an unbiased approach, first establishing the repertoire of evolutionarily conserved genes that show concordant expression changes across HD human and mouse striata and HD fly brains. We then integrated this comparative transcriptomic data with high-throughput *in vivo* behavioral screening to acquire insight into glial contributions to HD pathogenesis and identify disease-modifying targets that mitigate the HD phenotype.

Results

The HD transcriptome is conserved among evolutionarily distant model systems

To study the contributions of neurons and glia to HD pathogenesis, we first needed to define a transcriptomic signature that would enable us to move across species (human, mouse, and fly) (Figure 1A). We began with human tissue. Since the striatum is the brain region most prominently affected in HD, we compared the gene expression profiles of human post-mortem striatal samples from healthy individuals and patients with HD, from different stages of the disease (i.e., Vonsattel Grade 0-4) (Hodges et al., 2006; Vonsattel et al., 1985). We identified 1,852 downregulated and 1,941 upregulated differentially expressed genes (DEGs) in patients with HD compared to healthy individuals (Figure 1B).

We then reanalyzed published RNA-seq data from mouse striata, using an allelic series of knock-in mouse models with varying CAG-repeat lengths at six months of age (Langfelder et al., 2016). Because it is unclear which CAG tract length in mice most faithfully recapitulates HD pathogenesis, the triplet repeat length was treated as a continuous trait, and we narrowed our analysis to DEGs that correlate with increasing CAG repeat length. Comparing the striata of wild-type mice to the knock-in HD mouse models, there were 3,575 downregulated and 3,634 upregulated DEGs (Figure 1B). (The greater genome coverage provided by RNA-seq (Miller et al., 2014) yielded larger datasets for mouse and, below, for *Drosophila* than for humans.)

We performed RNA-seq leveraging *Drosophila* HD models (Kaltenbach et al., 2007; Romero et al., 2008) (see Methods) to compare the effect of expressing m*HTT* in either neurons or glia. The binary GAL4-*UAS* system was used to drive the expression of human m*HTT* either in neurons (*elav>GAL4)* or glia (*repo>GAL4)*. Both full-length (HTT^{FLQ200}) and N-terminal ($HTT^{NT231Q128}$) models were used in this set of experiments, since both the full protein and N-terminal HD fragments accumulate in the human brain as a result of proteolysis and mis-splicing (Kim et al., 2001; Neueder et al., 2017; Sathasivam et al., 2013; Wellington et al., 2002). Principle component analysis (PCA) showed that the greatest differences

between samples are attributable to the cell-specific drivers, and not to the use of N-terminal vs. full-length protein (Figure S1). Expressing m*HTT* in neurons resulted in 3,058 downregulated and 2,979 upregulated DEGs, while expressing m*HTT* in glia resulted in 3,127 downregulated and 3,159 upregulated DEGs. There were also DEGs common to both neurons and glia expressing m*HTT*: 1,293 downregulated and 1,181 upregulated (Figure 1B).

With these transcriptomic signatures in hand, we were able to compare gene expression profiles across the three species. We focused on genes with significantly altered expression (using a FDR<0.05; see Methods) in the same direction (i.e., upregulated or downregulated) in response to mHTT expression across these three species, including both *Drosophila* HD models. We call genes that meet this criterion concordantly altered DEGs (Table S1).

We compared DEGs using a graph-based approach (see Methods) that allows for evolutionary divergence and convergence, instead of imposing one-to-one relationships. 815 upregulated DEGs observed in HD patient-derived striatal tissue had an orthologous gene in the HD mouse model and at least one *Drosophila* model of HD that was concordantly upregulated. Similarly, 791 DEGs identified in HD patients had an orthologous gene in mouse and *Drosophila* models that was concordantly downregulated (Figure 1C). About 40% of the alterations in gene expression in patient striatal samples are concordant with orthologous genes in both *Drosophila* and mice models of HD. To determine whether this result could be an artifact of overlapping a large number DEGs in each model, we randomly selected and overlapped 815 and 791 orthologous genes across the three species 20,000 times. Based on the resulting distribution, we concluded that the overlap of concordant, orthologous DEGs across the various HD models was not random ($p=6.37x10^{-158}$ and $p=1.66x10^{-165}$, Probability Distribution Test).

To compare the consequence of expressing m*HTT* in glia versus neurons, we recalculated the overlaps between the three species, distinguishing DEGs from the neuron-only and glia-only HTT-expressing *Drosophila*. There were 425 concordantly upregulated and 545 concordantly downregulated DEGs in glia. We also found 522 upregulated DEGs and 453 downregulated specific to neurons. Out of these groups of DEGs, 310 were upregulated and 320 were downregulated in both neurons and glia. To acknowledge the proportion of transcriptional alterations we excluded by specifying concordant expression with the HD *Drosophila* models, we also calculated the overlap between concordant DEGs observed only in striata from HD patients and mice. We found that 83.7% of upregulated DEGs and 77.7% of downregulated DEGs that were altered concordantly in human and mouse HD striata were also concordantly altered in the brains of the neuronal and/or glial HD *Drosophila* models (Figure 1D). Of the genes that showed concordantly altered expression only in human and mouse striata, 64 (40%) of the upregulated and 68 (30%) of the downregulated DEGs did not have an ortholog in *Drosophila*.

Network analysis identifies biological processes disrupted by mHTT toxicity in glia

To investigate the cellular pathophysiology represented by DEGs in neurons and glia, we constructed protein-protein interaction (PPI) networks using the STRING-db database (Szklarczyk et al., 2015). The upregulated and downregulated networks of DEGs responding to m*HTT* expression in neurons or glia had a significant PPI enrichment compared to networks constructed from an equivalent number of random genes selected from a whole-proteome background (Table S2A). To control for potential artifacts that could arise from using the whole proteome background, we performed a more stringent analysis using only proteins that are found in the striatum (Al-Ramahi et al., 2018). Using average node degree and betweenness as proxies for connectivity, we found that the glial and neuronal networks show higher network connectivity than expected by random chance among proteins present in the striatum (Table S2B).

This high connectivity suggested that the networks are enriched in specific biological processes and/or pathways. We therefore clustered the glial mHTT response and neuronal mHTT response networks using the InfoMap random walks algorithm (iGraph Package for R and Python) (Rosvall and Bergstrom, 2007). Clusters that had fewer than four nodes were filtered out of subsequent analysis. The glial networks formed 23 and 24 clusters for upregulated and downregulated DEGs, respectively. Both the upregulated and downregulated neuronal networks formed 29 clusters. We applied this clustering method to the networks of randomly selected striatal proteins in order to determine the expected number of clusters for networks of a similar size. Both the glial and neuronal networks formed significantly more clusters than would be expected from random selection (Table S2B).

To gain insight into biological processes represented by each cluster, we queried the five most significantly enriched terms (FDR<0.05) using the GO Biological Process and Kyoto Encyclopedia of Genes and Genomes (KEGG) terms within each cluster (Table S3). A synthesis of these terms was used to identify clusters in both the glial and neuronal networks (Table S3, Figures S2B and S2C). We compared the membership within clusters across the glial and neuronal networks using a pair-wise hypergeometric test and identified fourteen clusters of upregulated DEGs common to both glial and neuronal networks. Similarly, there were fifteen clusters of downregulated DEGs common to the both networks (Figure S2A).

Given the aims of our study, the clusters of DEGs specific to glia (represented by nodes in Figure 2) were of particular interest to us. Six clusters were specifically upregulated in response to m*HTT* expression, enriched in genes involved in transcription and chromatin remodeling, amino acid metabolism, cell proliferation, cytokine signaling/innate immunity, arachidonic acid metabolism, and steroid synthesis (Figure 2A). Six clusters were downregulated in response to glial m*HTT* expression, containing genes involved in synapse assembly, calcium ion transport, immune system regulation,

phagocytosis, mRNA processing, and fatty acid degradation (Figure 2B).

We applied the same network analysis to genes that had concordantly altered expression in HD patient striata and HD mouse model striata but not in HD *Drosophila* models (Figure S3A). We observed that clusters comprising DEGs specific to the HD patients and the mouse models were functionally related to DEGs in both the glial and neuronal networks (Figure S3B).

Distinguishing glia-specific gene expression alterations from bulk tissue profiles

Gene expression data from bulk tissue does not provide the resolution required to define cell-autonomous gene expression alterations resulting from mHTT toxicity. Therefore, we compared DEGs (FDR<0.1) in human embryonic stem cells from individuals with HD (carrying 40-48 CAG repeats) with healthy embryonic stem cells that have been differentiated into either CD140+ oligodendrocyte progenitor cells (OPCs) or CD44+ astrocyte progenitor cells (APCs) (Osipovitch et al., 2019). We compared the resulting list of DEGs identified in the HD OPCs (1,439 genes) and HD APCs (193 genes) to the list of conserved HD DEGs from flies expressing m*HTT* in glia.

We identified 46 upregulated and 91 downregulated DEGs in common (Figure 3A). Astrocyte progenitor cells had 4 upregulated and 12 downregulated genes in common. We next asked whether any clusters in the fly glial networks were enriched in genes dysregulated in HD OPCs or APCs. The Synapse Assembly cluster (Figure 2B) was significantly enriched in genes with reduced expression in HD OPCs (Fisher's Exact Test, p<0.001), including *SYT13, LRRTM1, GRM1, EPB41L2, DLGAP3,* and *AGAP2*; the only gene of this cluster that was upregulated in HD OPCs was *NRXN3* (Figure 3B and 3C).

In sum, by using a comparative, network-based analysis of the HD transcriptome we associated dysregulation of several biological processes with the expression of m*HTT* in glia. Layering the gene expression profile of homogenous glial populations affected by mHTT onto these networks, we were able to extract from the bulk-tissue analysis a cluster of genes related to synaptic assembly that are altered in response to glial mHTT toxicity.

Downregulation of synapse assembly genes is compensatory in HD

The next question we sought to answer is whether changes in expression of synaptic assembly genes are compensatory or pathogenic. We reasoned that if lowering the expression of a downregulated HD DEG aggravated mHTT-induced toxicity, then the downregulation of that gene is pathogenic. Conversely, if reducing the expression of a DEG led to an improvement in HD-related phenotypes, we considered that reduction to be compensatory. We previously used this approach, which takes advantage of the genetic tractability of *Drosophila* and the availability of high-throughput behavioral screening as a proxy for neurological function, to discover modifier genes that reduce HTT protein levels in HD patient

cells (Al-Ramahi et al., 2018). Here we assessed the effect of various genetic changes in the same group of animals over time, following the expression of mHTT in either glia, neurons, or both cell types. We used a custom, robotic assay system which video-records flies climbing upwards to the top of a vial after being knocked to the bottom (negative geotaxis) to track the behavior of individual *Drosophila* in real time and measure several motor metrics including speed (see Methods). Healthy flies reliably climb to the top at a steady rate until the effects of aging gradually reduce their speed. In contrast, animals expressing mHTT specifically in glia or neurons show much more rapid, if still age-dependent, loss of climbing speed compared to animals expressing a non-targeting hairpin RNA (hpRNA). While we only focus on the effect of these genetic perturbations on speed, we also observe impairments in coordination, balance, and direction (output as number of turns and stumbles) in *Drosophila* expressing m*HTT* (data not shown).

The expression of *SYT13, LRRTM1, GRM1, EPB41L2, DLGAP3,* and *AGAP2* is reduced in HD OPCs derived from human embryonic stem cells (Osipovitch et al., 2019), which is consistent with the expression patterns we observed in patient-derived striatal tissue, knock-in mouse model striatal tissue, and in neuronal tissue from *Drosophila* expressing m*HTT* in glia (Figure 3C). We performed genetic perturbation analysis on the *Drosophila* orthologs of these genes to assess whether their downregulation was pathogenic or compensatory in glia. Diminishing expression of the *Drosophila* orthologs of these six genes mitigated the behavioral deficits induced by m*HTT* expression in glia (Figure 3D, additional controls in Figure S4B). We concluded that reduced expression of these genes is a compensatory response to m*HTT* expression in glia.

There were additional protein interactors in Synapse Assembly whose expression was not altered in the HD-affected OPCs or APCs compared with controls but which were nonetheless downregulated across all three HD models. In our behavioral assay, reducing expression of these interactors, including *NLGN3, NLGN4X, HOMER1,* and *SLITRK5,* was also protective against glial mHTT toxicity (Figure S4A, Table S4; additional controls in Figure S4B).

In sum, comparative transcriptomic analysis indicated that genes within the Synapse Assembly cluster are associated with the glial response to HD, and the high-throughput behavioral assay further defined this response as compensatory.

Decreasing Neurexin expression in glia mitigates mHTT-induced pathogenesis in both neurons and glia

NRXN3 was identified as a DEG in both our cross-species comparative transcriptomic analysis and in the gene expression profile of the HD glial progenitor population. *NRXN3* expression was lower in the bulk HD transcriptome across species compared to their respective controls, but it was more highly expressed in the HD OPCs than in controls. This discordance between the bulk and single-cell type gene expression profiles might be a result of time-dependent changes in gene expression as neurons age, but it

prevented us from classifying the *NRXN3* expression changes as being compensatory or pathogenic. We were particularly interested in neurexins, including NRXN3, because they mediate contact between pre- and post-synaptic neurons (Ushkaryov et al., 1992; Zeng et al., 2007).

We therefore asked whether downregulation of *Drosophila NRXN3* (d*NRXN3*, also known as nrx-1) is damaging or protective when both neurons and glia express m*HTT*. In the *Drosophila* behavioral assay, heterozygous loss of *dNRXN3* function in animals expressing m*HTT* in both neurons and glia mitigated mHTT toxicity and improved behavior (Figure 4A, left panel). Reproducing this experiment with flies expressing m*HTT* only in glia yielded the same benefit (Figure 4A, middle panel). The obvious next question, given its canonical role in neuron-neuron contact, was whether d*NRXN3* heterozygosity would protect against mHTT pathogenesis in neurons. Interestingly, the answer was no (Figure 4A, right panel). Consistent with this, glia-specific knockdown of d*NRXN3* (using the *repo-GAL4* driver) mitigated mHTT toxicity in glia (Figure 4B, left panel), but neuron-specific knockdown (using the *elav-GAL4* driver) of d*NRXN3* did not mitigate mHTT toxicity in neurons (Figure 4B, right panel). In sum, reducing d*NRXN3* in both neurons and glia protects against glial pathogenesis—and the combination of neuronal and glial pathogenesis—but not neuronal pathogenesis. This implies that mHTT disrupts some aspect of glial-neuronal interaction that is driven by the glia, since lowering expression of d*NRXN3* in glia is necessary and sufficient to mitigate behavioral impairments caused by m*HTT*.

To investigate whether *Nrxn3* is expressed in astrocytes in the striatum of HD mice, we performed *in situ* hybridization in coronal sections of striatal tissue taken from a mouse model of HD ($Hdh^{zQ175/+}$) to probe *Nrxn3* mRNA. *Nrxn3* was expressed in striatal astrocytes (Figure 4C and 4D). In conclusion, modulating the expression genes other than m*HTT* in glia could be an effective strategy for ameliorating HD-induced CNS dysfunction.

Reducing SERPINA1 function mitigates behavioral impairments in neurons and glia, and lowers mHTT protein levels

We were curious to identify modifiers that concordantly affect mHTT-induced pathogenesis in both neurons and glia, as these might be particularly attractive therapeutic targets for HD. We were particularly interested to discover whether any such shared modifiers exert their effect by reducing mHTT levels, which is considered a promising approach to therapy (Al-Ramahi et al., 2018; Barker et al., 2020; Caron et al., 2020; Li et al., 2019; Tabrizi et al., 2019; Wang et al., 2014; Wood et al., 2018; Yamamoto et al., 2000; Yao et al., 2015). We therefore again integrated network analysis with high-throughput experimentation.

Genes were sampled from both the neuronal and glial mHTT response networks by prioritizing those candidates with high centrality (calculated as a cumulative rank-score of node betweenness and

node degree) within each cluster. When available, we used alleles that perturb the expression or activity of the *Drosophila* orthologs in the same direction as the gene expression change in the HD patient population (Figure 5A). We screened 411 alleles, representing 248 *Drosophila* genes homologous to 211 human genes, for perturbations that improve the age-dependent behavior of *Drosophila* expressing m*HTT* in neurons or glia (Table S5). Alleles that ameliorated neuronal or glial function were verified in a subsequent trial in animals expressing m*HTT* across the CNS (in both neurons and glia). In all, we identified 25 genes with altered expression in HD that suppressed mHTT-induced behavioral deficits in neurons, glia, or both (Figure 5B and 5C, Figure S5A, Table S6).

In a secondary screen, we tested whether these disease modifiers common to both neurons and glia exerted their beneficial effects by lowering levels of the mutant HTT protein. We collected protein lysates from *Drosophila* expressing m*HTT* across the CNS that also bore alleles that suppressed mHTT-induced behavioral deficits in both neurons and glia. We assessed the quantity of mHTT protein in these lysates by western blot, comparing experimental (candidate modifiers) and control animals (carrying a non-targeting hpRNA). This secondary screen identified *Spn42De* as a modifier whose knockdown lowered mHTT levels. *Spn42De* is one of the four *Drosophila* homologues of human *SERPINA1* (which encodes alpha-1-antitrypsin, a member of a large group of protease inhibitors). *Spn42De*, human *SERPINA1* and mouse *Serpina1* are all upregulated in HD and they are part of the Wound Healing and Inflammation cluster in both the neuronal and glial mHTT response networks (Figure S2C). Knockdown of *Spn42De* (henceforth *dSERPINA1*) in *Drosophila* expressing m*HTT* in both neurons and glia mitigated behavioral impairments (Figure 6A). In independent immunoblots, *dSERPINA1* knockdown consistently reduced mHTT protein levels in lysates extracted from the heads *Drosophila* expressing m*HTT* in both neurons and glia (Figure 6B and 6C). As a control, we performed immunoblot analysis of lysates from a green fluorescent protein (GFP) reporter line to ensure that this allele of *dSERPINA1* did not reduce the function of the *GAL4-UAS* system (Figure S6).

To validate this observation across model systems we performed homogenous time-resolved fluorescence (HTRF) on $Hdh^{Q111/Q7}$ mouse striatal cell lysates that were treated with either a pool of non-targeting scramble siRNAs, a pool of siRNAs against *Htt*, or a pool of siRNAs against *Serpina1a* (the murine ortholog of *SERPINA1)*. *Serpina1a* knockdown significantly reduced mHTT signal (Figure 6D). Knockdown of *SERPINA1* thus protected against mHTT toxicity in neurons and glia by reducing levels of mutant HTT. Verifying this effect in multiple model organisms increases confidence in this observation and suggests that *SERPINA1* could potentially prove useful as a target for treating HD. Interestingly, *SERPINA1* expression is low in the healthy brain but it is upregulated in several disease conditions, consistent with a potential role in neuroinflammation (Abu-Rumeileh et al., 2020; Cabezas-Llobet et al., 2018; Gollin et al., 1992; Peng et al., 2015), and we previously showed that other genes in the subnetwork

implicated in neuroinflammation can be manipulated to lower mHTT protein levels (Al-Ramahi et al., 2018). *SERPINA1* may thus warrant investigation as a target for other neurological disorders as well.

Discussion

We found a high degree of overlap of differentially expressed genes (DEGs) across tissues from human HD brains, brains of HD mice, and flies that express m*HTT* in glia. This observation is consistent with previous evidence that *Drosophila* glia perform many of the same functions as mammalian astrocytes, oligodendrocytes, and microglia (Chung et al., 2020; Freeman and Doherty, 2006; Ziegenfuss et al., 2012). Several studies have also shown that wild-type glial cells ameliorate disease when transplanted into HD mice, and mHTT exerts a deleterious effect on glial development and function, which in turn influences HD pathogenesis (Benraiss et al., 2016; Bradford et al., 2009; Garcia et al., 2019; Huang et al., 2015; Osipovitch et al., 2019). More recently, it was discovered that transcription factors involved in glial differentiation and myelin synthesis are downregulated in glial progenitor cells (Osipovitch et al., 2019). Yet despite this progress, the overall contributions of glial genes to synaptic impairments and other key neurodegenerative pathologies remain poorly understood. The genetic malleability of *Drosophila* enabled us to thoroughly examine the neuron-glia interface from both the glial and the neuronal directions.

Synaptic dysfunction is a common theme among many neurodegenerative disorders (McInnes et al., 2018; Phan et al., 2017; Prots et al., 2018). While it is clear that the dysfunction of the glia-synapse interface is central to the pathophysiology of neurodegeneration (Filipello et al., 2018; Garcia et al., 2019; Lian et al., 2015; Litvinchuk et al., 2018), the underlying mechanisms remain underexplored relative to the interactions between pre- and post-synaptic neurons. Our results support the observation that the expression of m*HTT* in glia is sufficient to drive synaptic dysfunction (Wood et al., 2018). In HD, presynaptic motor neurons release elevated levels of glutamate into the synapse, driving medium spiny neurons (MSNs) into excitotoxicity (Estrada Sánchez et al., 2008; Hong et al., 2016). Hyperactivity of receptors at the post-synaptic densities sensitizes MSNs to excitotoxicity, further contributing to neurodegeneration (Estrada Sánchez et al., 2008). Astrocytic m*HTT* expression may contribute to neuronal excitotoxicity by elevating levels of glutamate, potassium, and calcium at the synapse (Garcia et al., 2019; Jiang et al., 2016; Tong et al., 2014).

Modifiers of mHTT-induced pathogenesis identified in our study, such as metabotropic glutamate receptors and the scaffold protein HOMER1, regulate calcium and glutamate signaling in astrocytes (Buscemi et al., 2017; Spampinato et al., 2018). Reducing the expression of these genes could prevent excess calcium and glutamate from accumulating at the synapse. Indeed, we previously found that HD neurons downregulate the expression of genes involved in calcium signaling in an effort to compensate

for HD pathogenesis (Al-Ramahi et al., 2018). Glial calcium signaling can also influence neuronal activity, however, at the neuronal soma (Weiss et al., 2019). In *Drosophila*, cortical glia modulate neuronal activity through potassium buffering, a process that is regulated by calcium-mediated endocytosis of potassium channels (Weiss et al., 2019). Glia can also physically disrupt synapses in disease states: Förster resonance energy transmission (FRET) *in vivo* revealed that, in HD, the distances between astrocytes and pre-synaptic neurons are increased at the cortico-striatal circuit (Octeau et al., 2018). Thus, knocking down the genes in the Synapse Assembly cluster could reduce physical interaction between glia and synapses, promoting normal synaptic function.

If in HD synapses grow more fragile and fewer in number as the disease progresses, why would down-regulating the expression of glial genes required for synapse formation and function be protective? We postulate it is for the same reason that downregulating calcium-signaling genes is compensatory (Al-Ramahi et al., 2018): the brain is attempting to protect against the excitotoxicity described above. Mutant HTT disrupts neuronal development (Ring et al., 2015) and skews embryonic neurogenesis toward producing more neurons (Barnat et al., 2020); by the time HD mutations carriers reach the age of six years, they have greatly enlarged striata and functional hyperconnectivity to the cerebellum (Tereshchenko et al., 2020). The more hyperconnected, the more abrupt the loss of these connections, and the more rapid the striatal atrophy that follows (Tereshchenko et al., 2020). The hyperfunction of a given brain region puts considerable strain on the circuit, and it seems that over the course of a lifetime, the brain keeps trying to compensate for the abnormalities that arise at different stages of HD. The recent observation that deletion of astrocytic neurexin-1α attenuates synaptic transmission but not synapse number supports this hypothesis (Trotter et al., 2020).

We do not think that the protection provided by modifiers in this cluster is limited to modulating neurotransmission. In astrocytes, calcium signaling also controls the activity of reactive astrocytes (Buscemi et al., 2017). Astrogliosis, or the proliferation of immune active astrocytes, is typically observed at later stages of HD (Al-Dalahmah et al., 2020; Buscemi et al., 2017). These immune-activated glia not only eliminate synapses (Liddelow et al., 2017; Sofroniew, 2009) but can also transmit mHTT aggregates through the synapse (Donnelly et al., 2020). In *Drosophila*, knockdown of *draper* prevents astrocytic phagocytosis and stops the spread of mHTT protein aggregates from pre-synaptic neurons to the post-synaptic compartment (Donnelly et al., 2020; Pearce et al., 2015). mHTT protein can also enter the synaptic space by endosomal/lysosomal secretion mediated by Syt7 (Trajkovic et al., 2017). In our present study, we observed that knockdown of synaptotagmins in *Drosophila* ameliorates glial mHTT-induced dysfunction. Thus, knocking down genes in the Synapse Assembly cluster could also benefit the circuit by reducing the transmission of aggregated mHTT protein from pre- to post-synaptic neurons.

Interestingly, loss-of-function variants in *NRXN1-3*, *NLGN1, NLGN3, DLGAP3* and *LRRTM1* have been associated with various disorders of synaptic dysfunction, including Autism Spectrum Disorder (ASD), schizophrenia, and obsessive compulsive disorder (OCD) (Nakanishi et al., 2017; Paris Autism Research International Sibpair Study et al., 2003; Südhof, 2008; Vaags et al., 2012; Wang et al., 2018; Windrem et al., 2017). We speculate that the consequences of loss of function of these genes depend on both dosage and context: modest reductions of gene expression can be protective in the context of HD pathogenesis, whereas a more severe loss of function results in ASD and OCD. Context could also relate to the affected cell-type. Future studies should investigate whether these loss of function variants associated with neurodevelopmental and psychiatric disorders alter the age of disease onset in patients with HD. It could be of particular interest to assess if these neurodevelopmental and psychiatric-associated variants prevent neurodevelopmental changes observed early in HD or blunt synaptic hyperactivity later in disease.

Acknowledgements

We thank Vicky Brandt for critical input on the manuscript. We also thank Steve Goldman for sharing data cited in this work and his thoughtful insight. This work was supported by grants to J.B. from NIH/ NIA (R01AG057339) and CHDI. B.L. is sponsored by Natural Science Foundation of China (31970747, 31601105, 81870990, 81925012). T.O. and M.M. were supported by the NIGMS Ruth L. Kirschstein National Research Service Award (NRSA) Predoctoral Institutional Research Training Grant (T32 GM008307) provided to the Genetics & Genomics Graduate Program at Baylor College of Medicine. A.L. was supported by Baylor College of Medicine Medical Scientist Training Program and the NLM Training Program in Biomedical Informatics and Data Science (T15 LM007093) at the Gulf Coast Consortium. The High Throughput Behavioral Screening core at the Jan and Dan Duncan Neurological Research Institute was supported by generous philanthropy from the Hildebrand family foundation. This project was also supported by the RNA In Situ Hybridization Core facility at Baylor College of Medicine with the expert assistance of Cecilia Ljungberg, Ph.D., and funding from a Shared Instrumentation grant from the NIH (S10 OD016167) and the NIH IDDRC Grant U54 HD083092 from the Eunice Kennedy Shriver National Institute Of Child Health & Human Development. The content is solely the responsibility of the authors and does not necessarily represent the official views of the Eunice Kennedy Shriver National Institute of Child Health & Human Development or the National Institutes of Health.

Author Contributions

J.B. conceived, supervised and provided resources for the study; Z.L. supervised bioinformatic studies; T.O., A.L., G.A., B.L., I.A.-R., Z.L. and J.B. contributed to experimental design; T.O., A.L., H.Z., R.K., H.K., J.W., M.M., A.P., M.H., H.W. Y.-W.W. performed experiments; T.O. and J.B. wrote the paper.

Declarations of Interest

The authors declare no competing financial interests.

Figures

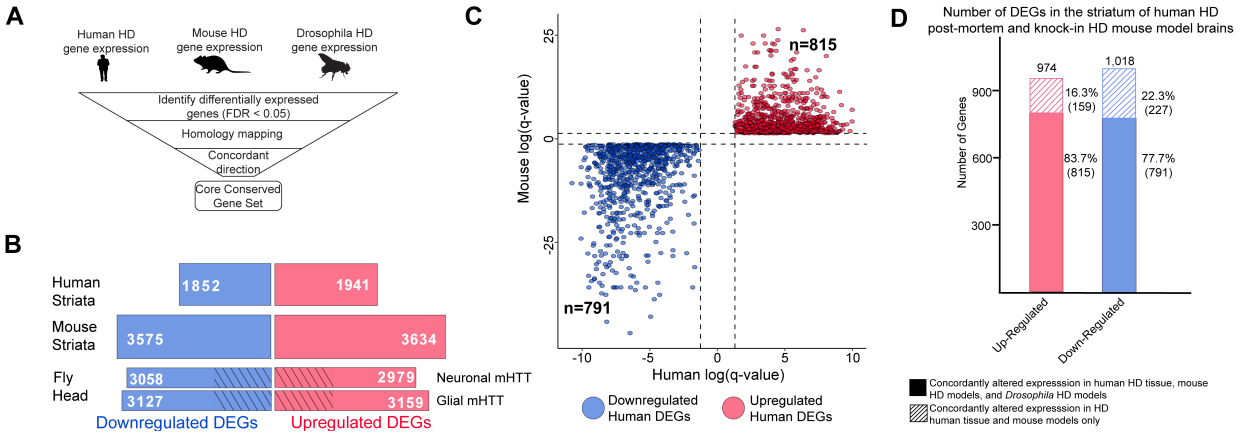

Figure 1. Differentially expressed genes (DEGs) in HD human striatal tissue are concordantly altered in mouse and *Drosophila* HD models.

A) Our approach to identifying orthologous genes in tissues from humans, mice, and *Drosophila* with concordant expression changes (i.e., upregulated or downregulated in all three systems) following m*HTT* expression.

B) The number of differentially expressed genes (DEGs) in each species-specific dataset that are downregulated (blue) or upregulated (red) (see Methods). *Drosophila* DEGs were from flies expressing either the N-terminal ($HTT^{NT231Q128}$) or full-length m*HTT* (HTT^{FLQ200}) in neurons (*elav-GAL4*) or glia (*repo-GAL4*). The DEGs in flies are grouped according to the cell type expressing m*HTT,* rather than mHTT model. The cross-hatched regions of the *Drosophila* bars represent DEGs shared between the neuronal and glial sets: 1,293 downregulated genes and 1,181 upregulated genes.

C) Points in the scatterplot represent human DEGs identified by the strategy outlined in (A) that are concordantly dysregulated across all three species. Red nodes represent upregulated DEGs (n=815), whereas blue nodes represent downregulated genes (n=791). The overlap of these concordant DEGs represents approximately forty percent of genes with altered expression in the human HD transcriptome that are upregulated ($p=6.37x10^{-158}$) or downregulated ($p=1.66x10^{-165}$). The p-value was calculated using a random background probability distribution over $2x10^5$ random samplings.

D) The stacked bar graph highlights that a large majority of concordant DEGs in human HD striata and knock-in HD mouse models are also concordantly altered in *Drosophila* models of HD.

Related to Figure 1, Figure S1: Expressing m*HTT* in *Drosophila* glia or neurons leads to distinct gene expression profiles. In contrast, the full-length and N-terminal models show relatively similar gene expression profiles.

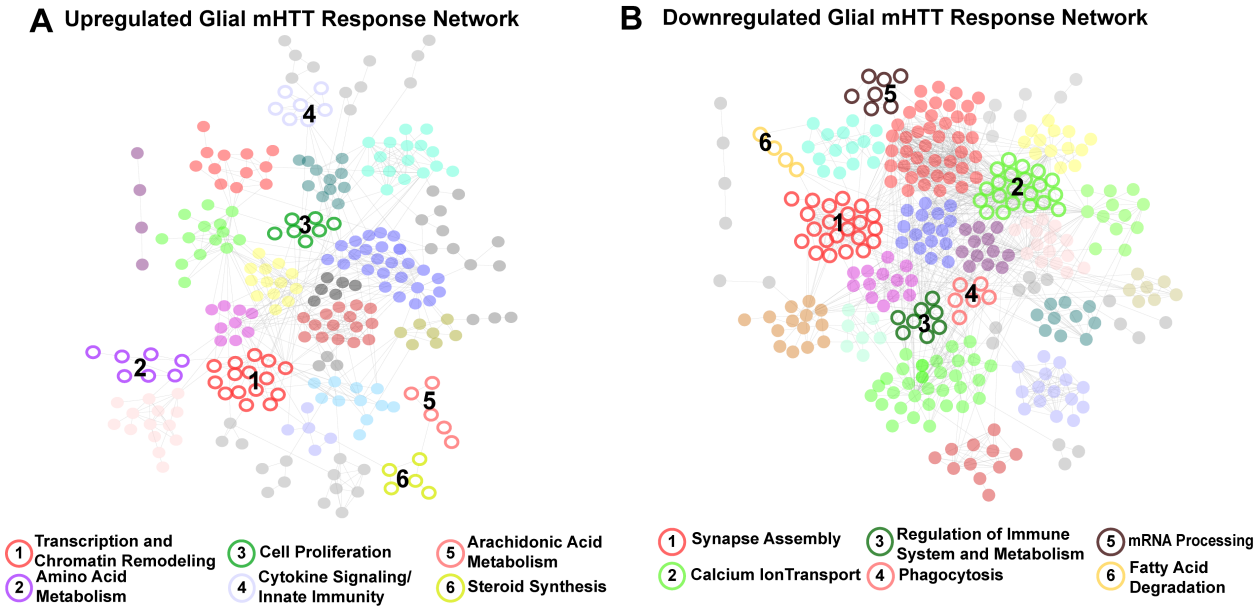

Figure 2. Clusters of concordant DEGs between human and mouse HD striata and *Drosophila* expressing mHTT in glia.

Clustered protein-protein interaction (PPI) networks of DEGs (STRING-db) that have higher (A) or lower (B) concordant expression in HD human tissue, an allelic series of knock-in HD mouse models, and *Drosophila* expressing m*HTT* ($HTT^{NT231Q128}$ or HTT^{FLQ200}) in glia. Clusters of DEGs (nodes) that were dysregulated in response to m*HTT* expression in glia are numbered and represented by open circles. Annotations listed below each network correspond to each numbered cluster and represent a synthesis of the top five most significantly enriched GO Panther Biological processes and Kyoto Encyclopedia of Genes and Genomes (KEGG) terms with an FDR<0.05 (**Table S3**). Nodes represented by solid circles were dysregulated in response to m*HTT* expression in glia but are also significantly similar in gene membership to clusters of DEGs in response to m*HTT* expression in neurons (**Figure S2**, hypergeometric test, $p<1x10^{-5}$).

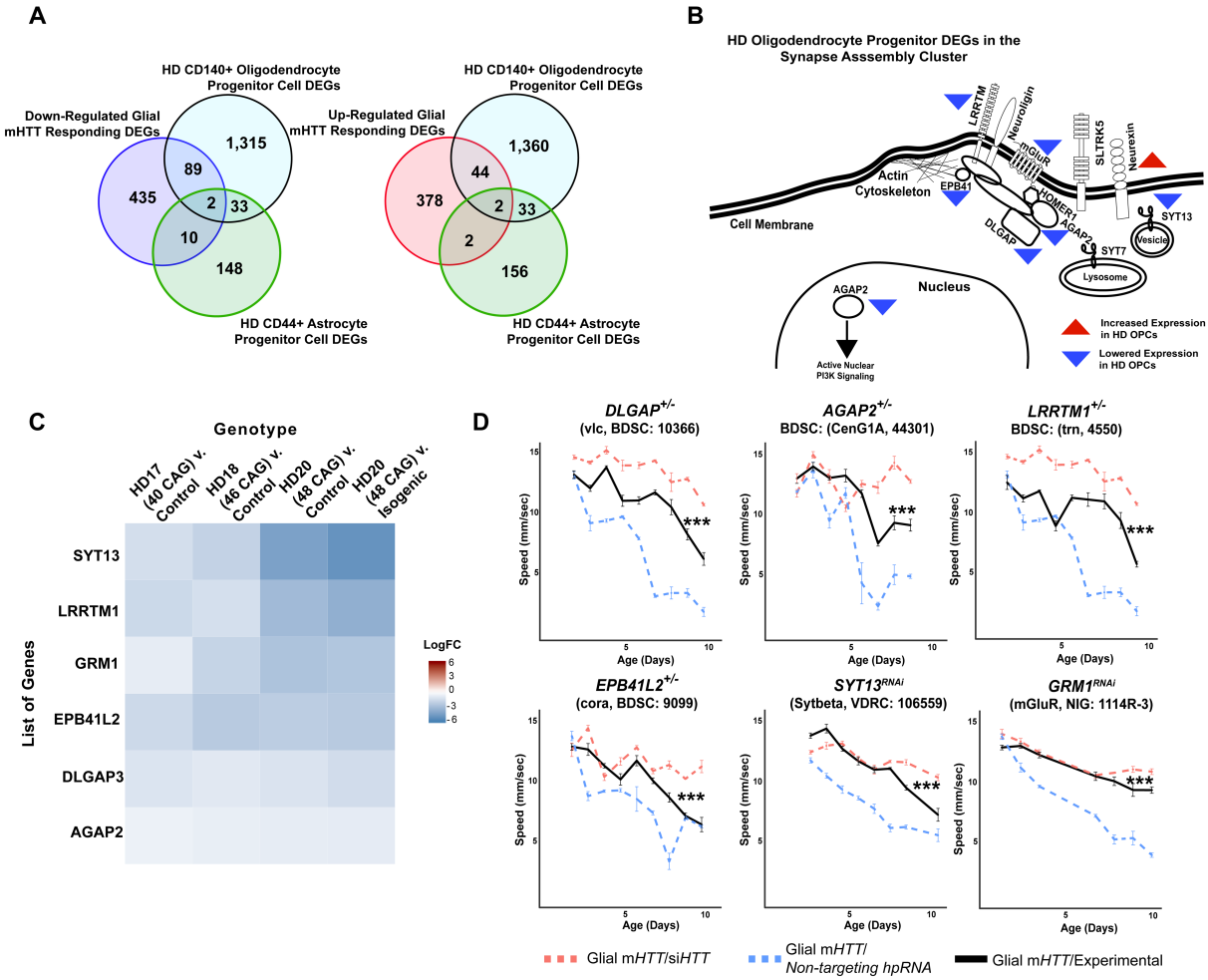

Figure 3. Reducing the expression of Synapse Assembly cluster genes in glia mitigates mHTT-induced behavioral impairments.

A) Overlaps between concordant DEGs from the cross-species analysis defined as responding to m*HTT* expression in glia and DEGs identified in HD human embryonic stem cells (hESCs) that have been differentiated into either CD140+ oligodendrocyte progenitor cells (OPCs) or CD44+ astrocyte progenitor cells (APCs) (Osipovitch et al. 2018).

B) Model placing Synapse Assembly cluster proteins into cellular context. The Synapse Assembly cluster was significantly enriched for DEGs in HD OPCs (Fisher's Exact Test, $p<0.001$). Only one gene, *NRXN3*, was upregulated in HD OPCs compared to controls (upward red triangle); the rest (*AGAP2*, *GRM1, LRRTM1*, *EPB41L2*, *DLGAP3*, and *SYT13*) were downregulated (downward blue triangles).

C) Heatmap representing genes with lower expression in HD OPCs compared to controls (presented as LogFC) that belong to the Synapse Assembly cluster. Each row is one downregulated gene; each column is a different HD human embryonic stem cell line, with CAG repeat length ranging from 40-48, compared to respective controls (Osipovitch et al 2018).

Figure 3 continued.

D) Behavioral assessment of fruit flies that express m*HTT* only in glia, after reducing the expression of the overlapping DEGs in HD OPCs and the Synapse Assembly cluster. Plots show climbing speed as a function of age. *** $p<0.001$ between positive control and experimental (by linear mixed effects model and post-hoc pairwise comparison (see Methods). Points and error bars on the plot represent the mean±SEM of the speed for three technical replicates. Each genotype was tested with 4-6 replicates of 10 animals. Modifying alleles in (D) are listed in the **Key Resources Table.** Additional climbing data for these genes can be found in **Figure S4A** and a summary of statistical analysis for this data can be found in **Table S4**. Control climbing data for these alleles can be found in **Figure S4B**.

Drosophila Genotypes: positive control (*w^{1118};UAS- non-targeting hpRNA/+; repo-GAL4,UAS-$HTT^{NT231Q128}$/+*), treatment control (*w^{1118}; repo-GAL4,UAS- $HTT^{NT231Q128}$/UAS-siHTT*), and experimental (*w^{1118}; repo-GAL4,UAS- $HTT^{NT231Q128}$/modifier*).

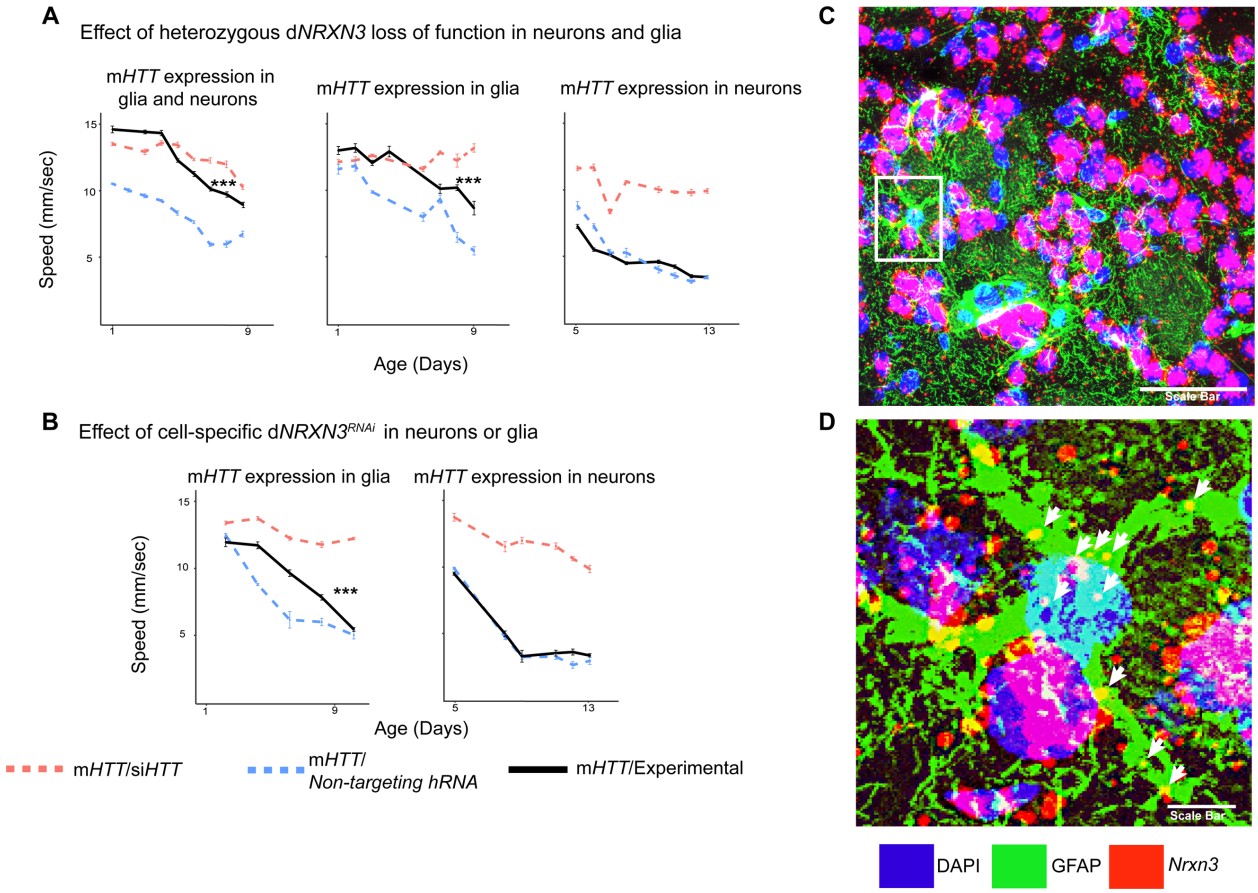

Figure 4. Glia-specific d*NRXN3* knockdown mitigates impairments caused by m*HTT* expression.

A) Behavioral assays (climbing speed as a function of age) showing that d*NRXN3* heterozygous loss-of-function (LOF) ameliorates behavioral impairments caused by expression of m*HTT* in both neurons and glia and in glia alone, but not in neurons alone.

B) Glia-specific d*NRXN3* knockdown mitigates behavioral impairments caused by m*HTT* expressed solely in glia; however, neuron-specific knockdown of *dNRXN3* does not affect impairments induced by m*HTT* expressed solely in neurons. *** <0.001 between positive control and experimental by linear mixed effects model and post-hoc pairwise comparison (see **Methods**). Points and error bars on the plot represent the mean±SEM of the speed for three technical replicates. Each genotype was tested with 4-6 replicates of 10 animals. A full summary of the statistical analysis for this data can be found in **Table S4**. Control climbing data for these alleles can be found in **Figure S4B**.

C) Astrocytes in the striatum of 6-month old knock-in HD mice ($Hdh^{zQ175/+}$) expressing *Nrxn3*. *In situ* probe for *Nrxn3* mRNA is in red (appears magenta when overlapping with the DAPI channel) astrocytes are immunostained using an antibody specific for glial fibrillary acidic protein (GFAP) in green, and DAPI in blue. Image was taken at 63x magnification using a Leica SP8 confocal microscope. Scale bar (in white on the bottom right) represents 50 µm.

Figure 4 continued.

D) Magnified image of the astrocyte highlighted in the white box in (C). White arrows indicate yellow puncta where *Nrxn3* mRNA localizes to astrocytes. Scale bar (in white on the bottom right) represents 5 µm.

Drosophila Genotypes: *dNRXN3* loss-of-function allele (y^1 *w*; Mi{*$y^{+mDint2}$*=MIC}nrx-1*^{MI02579}or *nrx-1*^{LOF}, BDSC: 61696), dNRXN3 RNAi allele (*UAS-nrx-1*^{hpRNA}, VDRC: 36326), neuronal and glial HD model with d*NRXN3* mutant (*elav*^{c155}*-GAL4/* y^1 *w*; repo-GAL4,UAS-HTT*^{NT231Q128}*/Experimental allele*), glial HD model with d*NRXN3* mutant (w^{1118}*/* y^1 *w*; repo-GAL4,UAS-HTT*^{NT231Q128}*/Experimental allele)*, and neuronal model with dNRXN3 mutant (*elav*^{c155}*-GAL4/* y^1 *w*; UAS-HTT*^{NT231Q128}*/Experimental allele)*.

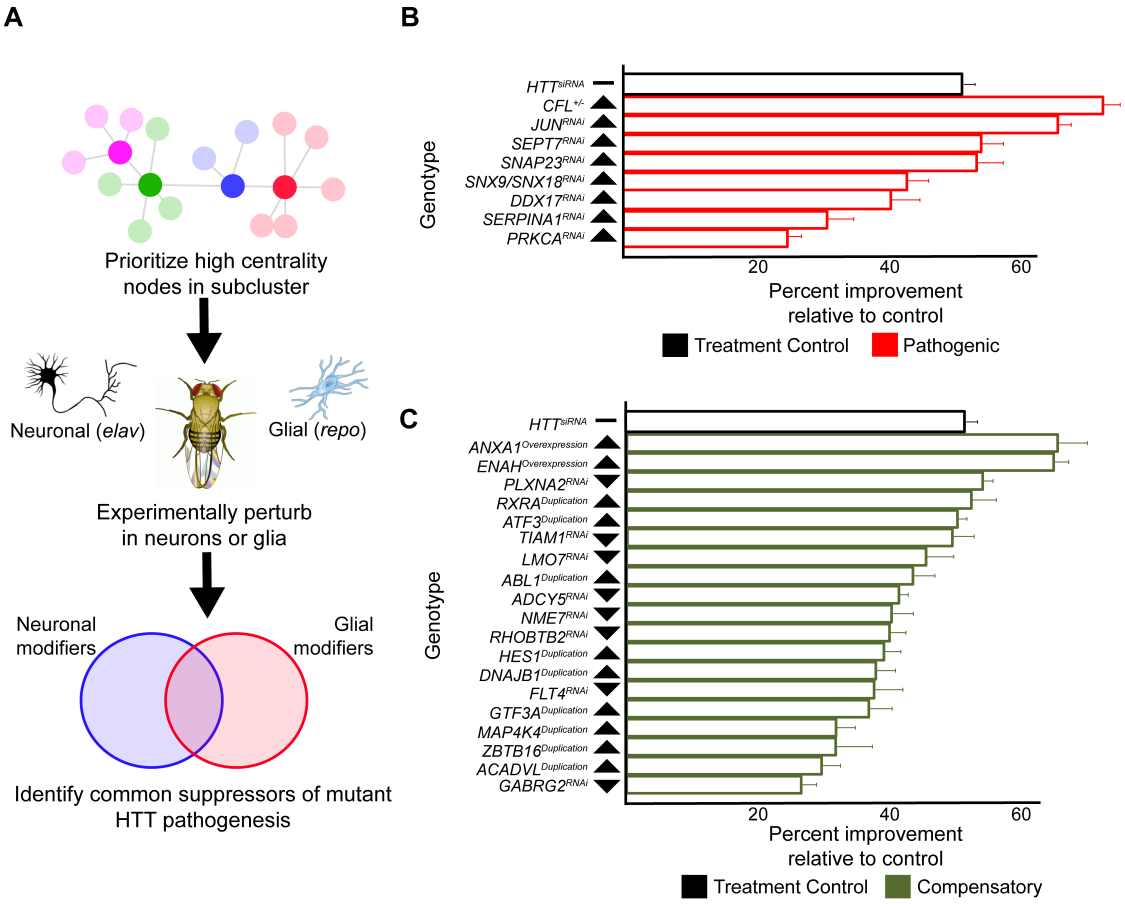

Figure 5. Compensatory and pathogenic gene expression changes shared by neurons and glia in response to m*HTT* expression.

A) Our approach for identifying modifiers of mHTT-induced behavioral impairments common to both neurons and glia. Genes that were central to their respective clusters were prioritized and manipulated in *Drosophila* expressing m*HTT* ($HTT^{NT231Q128}$) in either neurons (*elav-GAL4)* or glia (*repo-GAL4*).

B) Red bars represent the percent improvement in behavior over a 9-day trial, compared to positive control (non-targeting hpRNA) in *Drosophila* expressing *mHTT* in neurons and glia, after we antagonized pathogenic gene expression changes.

C) Green bars represent the percent improvement in behavior over a 9-day trial, compared to control (see B), after we mimicked compensatory gene expression alterations.

In (B) and (C), the top black bars represent the effect of directly targeting the m*HTT* transgene using an siRNA. Arrowheads indicate the direction of the conserved, concordant altered expression for each gene as a result of m*HTT* expression in humans, mice and *Drosophila*. Behavioral assay graphs corresponding to the data presented in (B) and (C) can be found in **Figure S5A**. Corresponding statistical analysis for

536 **Figure 5 continued.**

537 (B) and (C) can be found in **Table S6**. Corresponding controls for behavioral data can be found in **Figure**

538 **S5B and C**.

539 *Drosophila* Genotypes: Positive control (*elav^{c155}-GAL4/w^{1118};UAS- non-targeting hpRNA/+; repo-*

540 *GAL4,UAS-HTT^{NT231Q128}*/+), treatment control (*elav^{c155}-GAL4/w^{1118}; repo-GAL4, UAS- HTT^{NT231Q128}/UAS-*

541 *siHTT*) and experimental (*elav^{c155}-GAL4/w^{1118}; repo-GAL4, UAS- HTT^{NT231Q128}/modifier*).

542

543

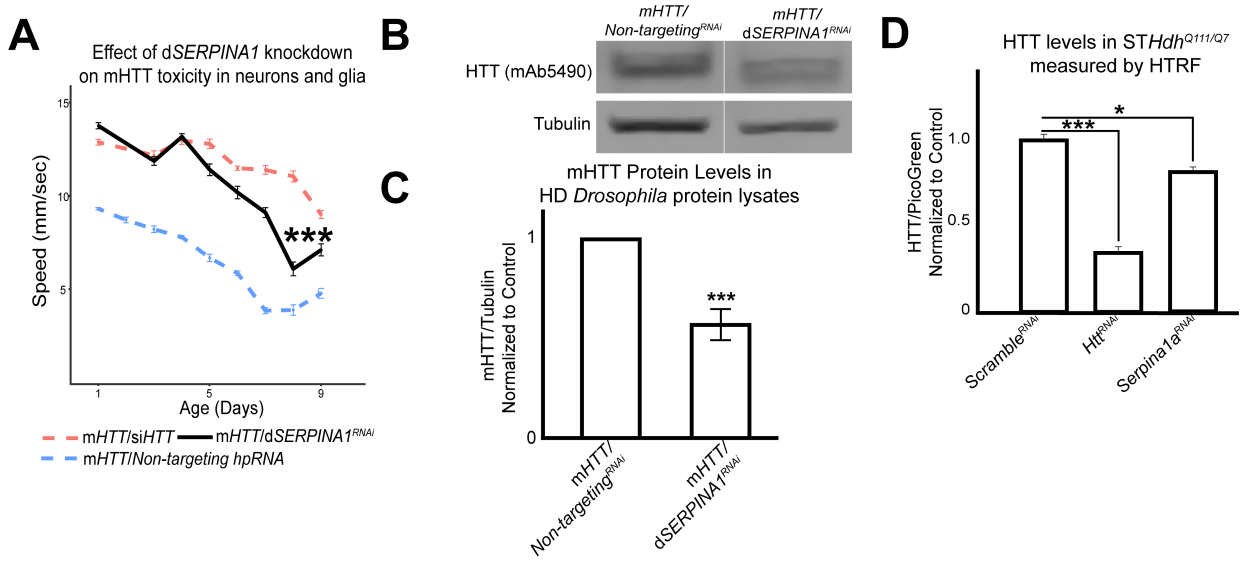

Figure 6. Antagonizing the pathogenic overexpression of *SERPINA1* in neurons and glia mitigates mHTT-induced behavioral impairments and lowers mHTT protein levels in *Drosophila* and HD mouse striatal cells.

A) Behavioral assays following knockdown of *dSERPINA1* in *Drosophila* expressing m*HTT* in neurons and glia. *** indicates p<0.001 by linear mixed effects model and post-hoc pairwise comparison between positive control and experimental animals. Points and error bars on the plot represent the mean±SEM of three technical replicates. Each genotype was tested with 4-6 replicates of 10 animals.

B) Representative western blot showing lower levels of mHTT following knockdown of *dSERPINA1* in *Drosophila* expressing m*HTT* in neurons and glia.

C) Quantification of five independent immunoblots showing the effect of *dSERPINA1* knockdown on mHTT levels in *Drosophila* head protein lysates. *** p<0.001 between positive control and d*SERPINA1* knockdown by one-way T-test.

D) Quantification of HTT protein levels in HD mouse striatal-derived cells (ST$Hdh^{Q111/Q7}$) measured by HTRF following treatment with a pool of scramble siRNAs (negative control), a pool of siRNAs against *Htt*, and a pool of siRNAs against *Serpina1a*. Quantification is presented as a ratio of the emission signal from the fluorescent D2 dye (HTT)/PicoGreen (number of cells per well). n=9 for each treatment group. * p<0.05 and *** p<0.001 between genotypes by Fisher's LSD test.

Drosophila Genotypes: *dSERPINA1* RNAi allele (*UAS-Spn42De*^{hpRNA}, VDRC: 102622), positive control (*elav*^{c155}*-GAL4/w*^{1118}*;UAS- non-targeting hpRNA/+; repo-GAL4,UAS-HTT*^{NT231Q128}/+), treatment control (*elav*^{c155}*-GAL4/w*^{1118}*; repo-GAL4, UAS- HTT*^{NT231Q128}*/UAS-siHTT*), and dSERPINA1 experimental (*elav*^{c155}*-GAL4/w*^{1118}*;UAS-Spn42De*^{hpRNA}*/+; repo-GAL4, UAS-HTT*^{NT231Q128}/+).

Materials and Methods

Lead Contact and Material Availability

Further information and requests for resources and reagents should be directed to and will be fulfilled by the Lead Contact, Juan Botas (jbotas@bcm.edu).

Drosophila models

We began with *Drosophila* models expressing either N-terminal human HTT ($HTT^{NT231Q128}$) or full-length (FL) HTT (HTT^{FLQ200}) (Kaltenbach et al., 2007; Romero et al., 2008). The mHTT was expressed using either a pan-neuronal (*elav*) or a pan-glial driver (*repo*). Mutant strains for screening were obtained from Bloomington Drosophila Stock Center, GenetiVision, and the Vienna Drosophila Resource Center. All strains were maintained at 18ºC in standard molasses, yeast extract, agar media until their experimental use. For RNA-sequencing, the full-length models were raised at 29ºC and the N-terminal models were raised at 28ºC. All behavioral experiments were performed on females raised at 28ºC.

In figure 3D, we used the following mutants to assess the effect of reduced expression of synaptic genes in mHTT animals on behavior: $UAS\text{-}non\text{-}targeting^{hpRNA}$ (Vienna *Drosophila* Resource Center, ID:13974), $CenG1A^{LOF}$ or $y^1w^*;Mi\{MIC\}CenG1A^{MI06024}$ (Bloomington *Drosophila* Stock Center, ID: 44301), vlc^{LOF} or $y^1w^{67c23};P\{w^{+mc}=lacW\}vlc^{k01109}/CyO$ (Bloomington *Drosophila* Stock Center, ID: 10366), trn^{LOF} or $y^1w^{67c23};P\{w^{+mc}=lacW\}trn^{S064117}/TM3,\ Sb^1\ Ser^1$ (Bloomington *Drosophila* Stock Center, ID: 4550), $cora^{LOF}$ or $P\{ry^{t7.2}=neoFRT\}43D\ cora^{14}/CyO$ (Bloomington *Drosophila* Stock Center, ID: 9099), $UAS\text{-}Sytbeta^{hpRNA}$(Vienna *Drosophila* Resource Center, ID:106559), and $UAS\text{-}mGluR^{RNAi}$ (National Institute of Genetics, Japan, ID: 11144-R3).

To generate *Drosophila* that expressed a small interfering RNA that knocked down human *HTT* (*UAS-siHTT*), we cloned a 378bp inverted EcoRI, XbaI fragment of N-terminal Htt into the pMF3 vector (*Drosophila* Genome Resource Center). This fragment maps to base pairs 406 to 783 of the human mRNA *Huntingtin,* which we cloned using the following primers:

Forward 5'-gaattcGCACCGACCAAAGAAAGAAC-3'

Reverse 5'-tctagaGGCAGAAGGTTCACCAGGTA-3'

We first digested the PCR product with EcoRI and ligated it with itself to obtain inverted repeats. We then digested the inverted repeat with XbaI and pasted the fragment into the pMF3 vector (also cut with XbaI); the resulting plasmid was injected into *Drosophila* embryos using standard methods (Dietzl et al., 2007). We validated that this line lowers mHTT levels.

STHdh$^{Q111/Q7}$ mouse striatal cells

Immortalized mouse striatal cells heterozygous for m*HTT* (*STHdh$^{Q111/Q7}$*) were obtained from Coriell Cell Repositories (Camden, NJ) and cultured in DMEM (Life Technologies, cat. no. 11965) supplemented with 10% fetal bovine serum (Life Technologies, cat. no. 10082–147).

DEG identification in Drosophila *HD models*

We performed RNA-seq on head tissue collected from *Drosophila* expressing N-terminal (*UAS-HTT^{NT231Q128}*) or full-length (*UAS-HTT^{FLQ200}*) human mHTT in neurons (*elav-GAL4*) or glia (*repo-GAL4*). For each combination of HD model and driver, RNA-seq was performed at three time points to capture the early, middle, and late phases of disease pathogenesis, corresponding to behavioral deficits caused by mHTT-induced neuronal or glial dysfunction. At each timepoint, samples for HD and age-matched controls were collected in triplicate. *Drosophila* expressing the N-terminal construct and corresponding controls were obtained at 7,9, and 11 days post-eclosion for the neuronal driver, and at 5, 7, and 8 days post-eclosion for the glial driver. *Drosophila* expressing the full-length construct, samples were obtained at 18, 20, and 22 days post-eclosion for both the neuronal and glial driver. For RNA-seq the neuronal N-terminal, glial N-terminal, and glial full-length model *Drosophila* were raised at 28ºC. The neuronal full-length model *Drosophila* were raised at 29ºC. For each genotype at each timepoint, we collected an equivalent number of control animals (*elav-GAL4* or *repo-GAL4*) that were raised in the same conditions.

Three replicates of 50 virgin females were collected for each genotype and timepoint. Animals were aged in the appropriate temperature and were transferred to fresh food daily until tissue was harvested. At the selected ages, animals were transferred to 1.5ml tubes, flash frozen in liquid nitrogen, vigorously shaken and then sieved to collect 50 heads/genotype/replica (~5mg tissue/replica). Total RNA was extracted using the miRNeasy Mini Kit (Qiagen Cat. # 210074).

RNA-seq profiling and preprocessing was performed by Q2 Solutions (Morrisville, North Carolina). Samples were converted into cDNA libraries using the Illumina TruSeq Stranded mRNA sample preparation kit (Illumina Cat. #20020595) and were sequenced using HISeq-Sequencing-2x50bp-PE. Initial analysis was performed using Q2 Solution in-house mRNAv7 pipeline with a median of 49 million actual reads. After adapter sequences were removed, the reads were aligned to the *Drosophila melanogaster* transcriptome using Bowtie version 0.12.9 (Langmead and Salzberg, 2012). Expression was quantified using RSEM version 1.1.19, resulting in a median of 11,214 genes and 18,604 isoforms detected (Li and Dewey, 2011).

Homology mapping of HD DEGs by network-based intersection

Three homology maps were constructed to define conserved genes that were concordantly

dysregulated in response to mHTT toxicity: a *Drosophila*-human map, a *Drosophila*-mouse map, and a mouse-human map. The *Drosophila*-human map and *Drosophila*-mouse map were both obtained from DIOPT version 6.0.2 (Hu et al., 2011). To capture homology that results from evolutionary convergence and divergence we included lower DIOPT scores between *Drosophila* and mammals, instead of fitting one-to-one mappings between these species. The mouse-human homology mapping was obtained from the Mouse Genome Informatics (MGI) database hosted by Jackson Laboratories (Blake et al., 2017).

We integrated these three homology maps by representing each map as an undirected bipartite graph, where nodes are genes of one species and edges represent homology between two genes across species. All components were then merged to form an undirected graph where each node represents a gene name and corresponding species. We applied this integrated homology map consisting of nodes representing the *Drosophila*, mouse, and human dysregulated genes, and all edges induced by the corresponding nodes, to obtain a subgraph consisting of multiple connected components. If any individual connected component contained nodes that belong to all three species, we characterized all genes within the connected component as concordant.

Protein-protein interaction network and clustering

To examine how the upregulated and downregulated core genes interact functionally, we used STRING v10.5 (Szklarczyk et al., 2015). Only high-confidence interactions (edge weight > 0.7) were considered. Each node is converted from an ENSEMBL ID to human Entrez ID via the provided mapping file (v10, 04-28-2015). Four subgraphs of STRING were then induced on each core gene set separately. Nodes were further clustered with the InfoMap community detection algorithm (Rosvall and Bergstrom, 2008), implemented in the Python iGraph package, with the default settings (trials = 10) (Csardi and Nepusz).

Drosophila behavioral assay

We crossed female virgins that carried the mutant HTT (mHTT) transgene under the control of either the neuronal or glial driver, or the cell-specific driver alone, to males carrying the experimental allele. We introduced a heat-shock-induced lethality mutation on the Y chromosome ($Y^{P\{hs\text{-}hid\}}$) to the disease and cell-specific driver stocks to increase the efficiency of virgin collection (Starz-Gaiano et al., 2001). For crosses involving alleles that were lethal or sterile mutations on the X chromosome, this mating strategy was reversed. For behavioral assays, *elav>*$HTT^{NT231Q128}$ and *repo>* $HTT^{NT231Q128}$ animals were raised and maintained at 28.5ºC. *Elav,repo>*$HTT^{NT231Q128}$ animals were raised and maintained at 25ºC.

The negative geotaxis climbing assay was performed using a custom robotic system (SRI

International, available in the Automated Behavioral Core at the Dan and Jan Duncan Neurological Research Institute). The robotic instrumentation elicited negative geotaxis by "tapping" *Drosophila* housed in 96-vial arrays. After three taps, video cameras recorded and tracked the movement of animals at a rate of 30 frames per second for 7.5 seconds. For each genotype, we collected 4 to 6 replicates of 10 animals to be tested in parallel. Each trial was repeated three times. The automated, high-throughput system is capable of assaying 16 arrays (1,536 total vials) in ~3.5 hours. To transform video recordings into quantifiable data, individual *Drosophila* were treated as an ellipse, and the software deconvoluted the movement of individuals by calculating the angle and distance that each ellipse moves between frames. The results of this analysis were used to compute more than two dozen individual and population metrics, including distance, speed, and stumbles.

Software required to run and configure the automation and image/track the videos include: Adept desktop, Video Savant, MatLab with Image Processing Toolkit and Statistics Toolkit, RSLogix (Rockwell Automation), Ultraware (Rockwell Automation). Additional custom designed software includes: Assay Control – SRI graphical user interface for controlling the assay machine; Analysis software bundles: FastPhenoTrack (Vision Processing Software), TrackingServer (Data Management Software), ScoringServer (Behavior Scoring Software), Trackviewer (Visual Tracking Viewing Software).

In situ *and immunofluorescence in HD mouse brain sections*

mRNA in situ hybridization (ISH) and immunofluorescence were performed on 25-µm thick coronal brain sections cut from fresh-frozen brain harvested from a 6-month old $Hdh^{zQ175/+}$ mouse. We generated digoxigenin (DIG)-labeled mRNA antisense probes against *Nrxn3* using reverse-transcribed mouse cDNA as a template and an RNA DIG-labeling kit from Roche (Sigma). Primer and probe sequences for the *Nrxn3* probe is available in Allen Brain Atlas (http://www.brain-map.org). ISH was performed by the RNA In Situ Hybridization Core at Baylor College of Medicine using an automated robotic platform as previously described (Yaylaoglu et al., 2005) with modifications of the protocol for fluorescent ISH. In brief: after the described washes and blocking steps, the DIG-labeled probe was visualized using a tyramide-Cy3 Plus kit (1:50 dilution, 15-minute incubation, Perkin Elmer). Following washes in phosphate buffered saline (PBS) the slides were stained with 1:500 anti-GFAP rabbit polyclonal antibody (DAKO, Z0334) diluted in 1% blocking reagent in Tris buffered saline (Roche Applied Science, 11096176001) overnight at 4ºC. After washing, slides were treated with 1:500 anti-rabbit IgG Alexa 488 secondary antibody for 30 min at room temperature (Invitrogen, A-11008). The slides were stained with DAPI and cover slipped using ProLong Diamond (Invitrogen, P36970). Images were taken at 63x magnification using a Leica SP8 confocal microscope.

Immunoblot of Drosophila lysates

For all immunoblot experiments, *Drosophila* were raised and maintained at 25ºC. Female F1 progeny were collected and flash-frozen 24 hours after eclosion. Heads were separated by genotype and divided into 8 individuals per replicate. *Drosophila* heads were lysed and homogenized in 30uL of lysis buffer (1x NuPage LDS Sample Buffer, 10% beta-mercapethanol) and boiled at 100 ºC for 10 minutes. Lysates were loaded on a 4-12% gradient Bis-Tri NuPage (Invitrogen) gels and run at a constant voltage of 80V for an hour and then 120V for 30 minutes. For mHTT levels, a 20% methanol transfer buffer was used to transfer proteins at 4ºC overnight using a 200mA current. For mCD8::GFP, proteins were transferred using a 10% methanol buffer for 2 hours at 4ºC a 200mA current.

Prior to antibody treatment, all membranes were treated with blocking solution (5% non-fat milk in 1x TBST). For primary antibody treatment all antibodies were diluted in blocking solution. To assess mHTT levels, membranes were the treated with a 1:500 mouse anti-HTT solution (mAb5490, EMD Millipore) overnight. For a loading control, membranes were subsequently treated with a 1:1000 alpha-tubulin antibody (Abcam EP1332Y). 1:1000 Rabbit anti-GFP (ThermoFisher A-11122) was used to assess levels of mCD8::GFP, and 1:1000 anti-lamin C (Hybridoma Bank LC28.26) was used as a loading control. All blots were treated with 1:5000 Goat anti-Mouse (IRDye® 800CW Goat anti-Mouse IgG) and Goat anti-Rabbit (RDye® 680RD Goat anti-Rabbit IgG) secondary antibodies diluted in blocking solution for 1 hour and imaged using the Odyssey CLx imager (LI-COR Biosciences).

Knockdown of Serpina1a *and homogenous time-resolved fluorescence in STHdh$^{Q111/Q7}$ cells*

ST*Hdh*$^{Q111/Q7}$ cells were reverse transfected with pooled small interfering RNAs (siRNAs) using Lipofectamine 2000 (Life Technologies, cat. no. 11668). Cells were treated with a pool of four small siRNAs per gene with the following sequences (Qiagen 1027280):

- *Htt*

1. 5’- GAAAUUAAGGUUCUGUUGA-3’
2. 5’- CCACUCACGCCAACUAUAA-3’
3. 5’- GAUGAAGGCUUUCGAGUCG-3’
4. 5’- UAACAUGGCUCAUUGUGAA-3’

- *Serpina1a*

1. 5’- GAAUAUAACUUGAAGACAC-3’
2. 5’-GGGCUGACCUCUCCGGAAU-3’
3. 5’- UGGUAGAUCCCACACAUAA-3’
4. 5’- GAAAGAUAGCUGAGGCGGU-3’

- *Scramble*

Following siRNA treatment, cell lysis buffer (1X phosphate buffered saline (PBS) with 1% TrintonX-100 and 1% EDTA-free protease inhibitor (Calbiochem, #539134)) was added to each well and the plate was put on ice for 30 minutes. After incubation, cells were homogenized and lysates were extracted. Separately, HTRF assay buffer was prepared using 50 mM NaH2PO4(pH7.4), 400 mM KF, 0.1% bovine serum albumin (BSA), 0.05% Tween-20 and Quant-ITTM Picogreen(1:1500). The donor antibody, 2B7 conjugated to terbium, was diluted in HTRF assay buffer to a concentration 0.023 ug/mL of and the acceptor antibody, mAb2166 (SigmaAldrich) conjugated to fluorescent dye D2, was diluted for a final concentration of 1.4 µg/mL. 5 µl of the HTRF buffer was added to 5uL of cell lysates (5 µl) in each well of a 384-well plate. Lysates were then incubated at 4ºC overnight.

HTRF was performed in a PerkinElmer EnVision multilabel plate reader (model #2104), measuring the 615nM and 665nM, as well as the Picogreen signal at 485nM. Each sample was measured following 30 cycles of the excitation at an interval of 16.6 ms.

DEG identification in Drosophila *HD models*

Differential expression analysis used the DESeq2 R package on a total of twelve comparisons (two HD models, two cell-specific drivers, and three timepoints) (Love et al., 2014). Outlier detection was performed using principle component analysis on normalized gene expression data, resulting in one sample being removed. To establish a list of upregulated and downregulated DEGs in *Drosophila*, we examined the false discovery rate (FDR) at every time point in both genetic models. If the FDR was less than 0.05 at any data point in the HD models compared to control, we established that that gene was dysregulated due to the presence of mHTT in either neurons or glia. We did not take the magnitude of fold-change into account, only the direction (upregulated or downregulated) (Langfelder et al., 2016).

Reanalysis of HD patient-derived and knock-in mouse model transcriptomes

The identification of DEGs from humans was based on microarray data from brain tissue collected post-mortem in patients with HD and age-matched, healthy individuals. For consistency with the reported results, we examined the summary statistics of the caudate probe on the Affymetrix U133 A and B microarrays. We computed the FDR by applying the Benjamini-Hochberg procedure to the p-values reported in Hodges et al. 2006. A probe was said to be dysregulated if the absolute value of its Fold Change was greater than 1.2 (or $\log_2$FC >0.263) and the FDR was less than 0.05. Since multiple Affymetrix probes can match to the same Entrez ID, we specified if that an Entrez-identified human gene was dysregulated, if there exists a matching probe that is also dysregulated.

We established lists of upregulated and downregulated DEGs in mice from RNA-seq data presented

in Langfelder et al. (Langfelder et al., 2016), where the authors profiled mRNA of an allelic series in a HD knock-in mouse model. We reanalyzed data from the striatum at 6 months, identifying gene expression alterations with that were significant (FDR < 0.05) in the continuous-Q case, a summary regression variable derived from DESeq that tests the association of the expression profile with Q-length as a numeric variable (Love et al., 2014).

Connectivity of the mHTT responding networks compared to a striatal proteome background

We randomly sampled 471 proteins (equivalent to the average number of input proteins in the mHTT Responding networks) 1,000 times, from 15,884 proteins that are expressed in the striatum. Implementing the same parameters that were used for the mHTT responding networks, we constructed clustered PPI networks with the random striatal protein lists as inputs. We calculated the average node degree and average node betweenness within each network of random genes and compiled a distribution using these results. A Z-score was calculated using the distribution compiled from the random striatal networks. These Z-scores were then used to calculate the p-values that were reported in Supplemental Table 2. All simulations and statistical calculations were performed in R.

Analysis of behavioral screen in Drosophila

We assessed behavior in *Drosophila* as the speed at which individual animals within one vial moved as a function of age and genotype using a non-linear random mixed effects model regression. Specifically, we looked at differences in regression between genotypes with time (additive effect, represented by a shift in the curve) or the interaction of genotype and time (interactive effect, represented by a change in the slope of the curve). We reported p-values representative of the pairwise post-hoc tests for testing whether all possible pairs of genotype curves are different in both models. We considered differences between positive controls and experimental perturbations of $p<0.001$ to be significant. P-values were adjusted for multiplicity using Holm's procedure. Code for this analysis is available upon request from the Botas Laboratory. All graphing and statistical analyses were performed in R.

Statistical analysis for western blot and homogenous time-resolved fluorescence

Images of western blots were analyzed using the Image Studio Lite software. We used an equivalent area to measure signal intensity across all replicates. We present proteins of interests as a ratio of the target protein to loading control. Experimental replicates were compared to controls using a one-sided Student's T-Test. For HTRF, levels of mHTT were calculated by taking the ratio of the fluorescence signals (665nM/615nM) and normalizing to the Picogreen signal in experimental groups after subtracting the signal from wells containing only sample buffer and HTRF buffer, without protein lysates. Results are

presented as the average and standard error of the mean of the ΔF (%) (ΔF (%) =(Sample ratio − blank ratio) /blank ratio× 100). P-values were calculated using Fisher's LSD test.

Data and Software Availability

Raw data from *Drosophila* and mouse ST*Hdh*$^{Q111/Q7}$ analysis available upon request. RNA-sequencing from the HD *Drosophila* models is available in NCBI GEO under accession GSE157287. Code for analysis of *Drosophila* behavioral assay in R available upon request.

Supplemental Figures

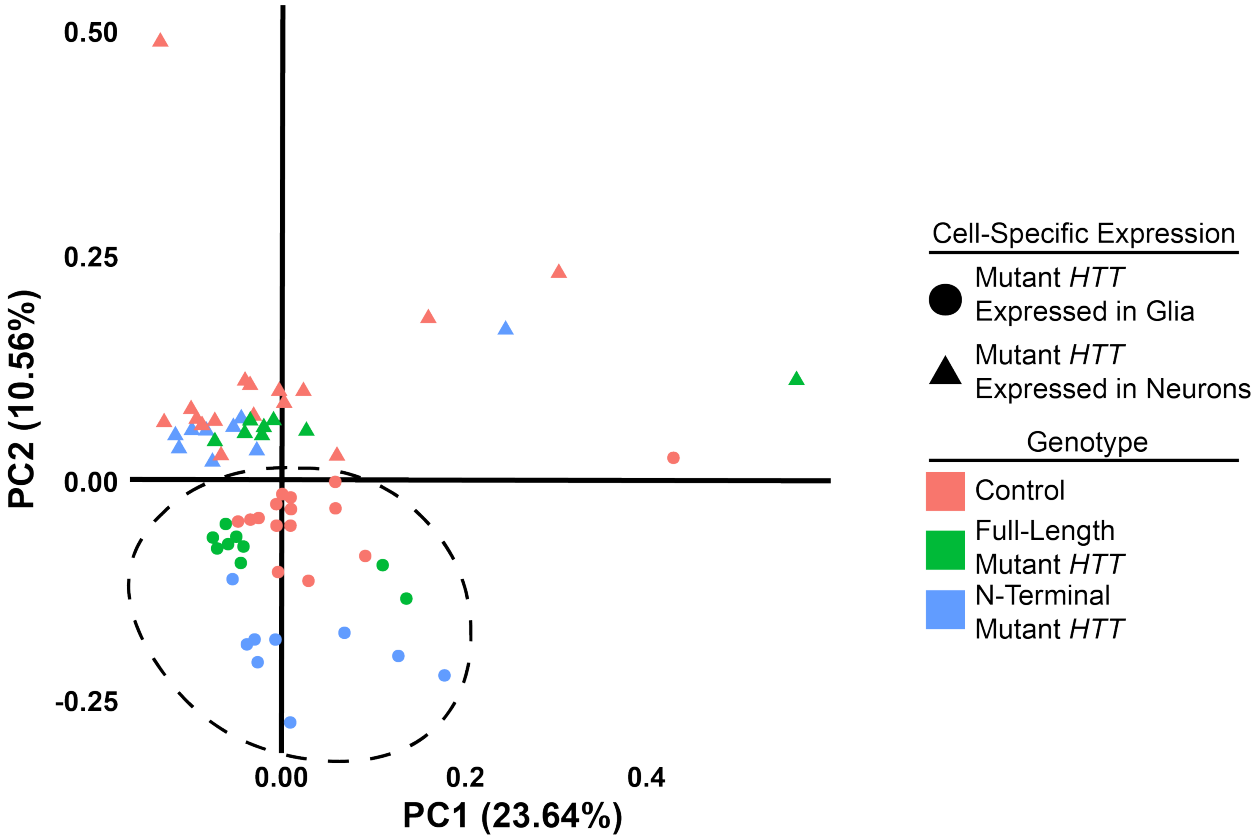

Supplemental Figure 1. Expressing m*HTT* in *Drosophila* glia or neurons leads to distinct gene expression profiles. In contrast, the full-length and N-terminal models show relatively similar gene expression profiles, Related to Figure 1.

Principal component analysis (PCA) plot of RNA-sequencing samples. Circles represent samples with transgenic expression in glia (*repo-GAL4*), while triangles represent samples transgenic expression in neurons (*elav-GAL4*). Red points represent control w^{1118} controls, green points represent animals expressing the full-length protein m*HTT* transgene (HTT^{FLQ200}), and blue points represent animals expressing the N-terminal m*HTT* fragment transgene ($HTT^{NT231Q128}$). Outliers skew the first component on the x-axis (23.64% of the variability). Samples expressing m*HTT* in glia separate from those expressing it in neurons along the second component on the y-axis (10.56% of the variability; dashed circle).

A

Whole proteome background

	m*HTT* expressed in neurons		m*HTT* expressed in glia	
	Up	Down	Up	Down
Input proteins	521	452	424	536
Edges	889	993	589	1410
PPI enrichment	<2E-16	<2e-16	1.63E-12	<2E-16

B

Striatal background

	m*HTT* expressed in neurons		m*HTT* expressed in glia	
	Up	Down	Up	Down
Average degree enrichment in striatum	1.01E-06	9.68E-08	1.17E-03	3.37E-15
Average betweenness enrichment in striatum	3.44E-06	3.63E-03	3.23E-03	5.11E-04
Number of clusters enrichment in striatum	3.09E-06	3.09E-06	1.23E-02	4.31E-03

Supplemental Table 2. Network connectivity of DEGs responding to glial or neuronal m*HTT* expression, Related to Figure 2.

Protein-protein interaction (PPI) networks (STRING-db) built from HD DEGs are significantly more connected (Probability Distribution Test) than networks of equivalent size built from proteins selected randomly out of a whole proteome (A) or striatal (B) background. HD DEGs are concordantly upregulated or downregulated in HD human striatal tissue, knock-in HD mouse striatal tissue, and tissue taken from *Drosophila* expressing m*HTT* in neurons or glia.

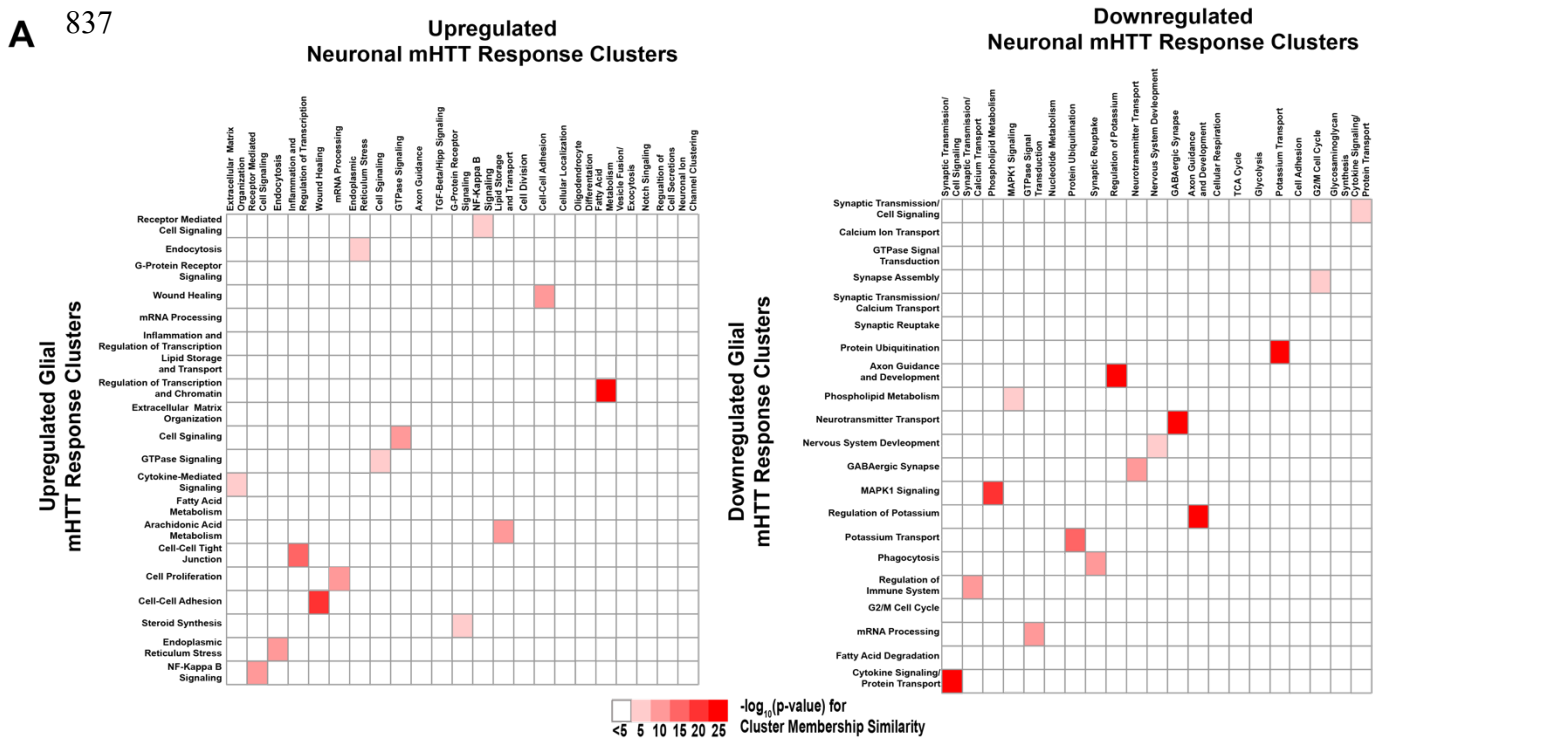

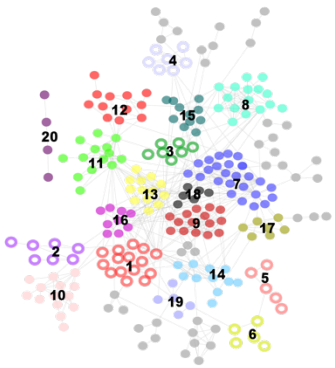

Clusters Upregulated in Response to mHTT in Glia Only

1. Transcription and Chromatin Remodeling
2. Amino Acid Metabolism
3. Cell Proliferation
4. Cytokine Signaling/ Innate Immunity
5. Arachidonic Acid Metabolism
6. Steroid Synthesis

Clusters Upregulated in Response to mHTT in Neurons or Glia

7. Receptor Mediated Cell Signaling
8. Endocytosis
9. G-Protein Coupled Receptor Signaling
10. mRNA Processing
11. Wound Healing and Inflammation
12. Extracellular Matrix Organization and Signaling
13. Inflammation/Regulation of Transcription
14. Lipid Transport and Storage
15. GTPase Signaling/ Actin Cytoskeleton
16. Cell Signaling
17. Fatty Acid Metabolism
18. Cell-Cell Adhesion
19. Endoplasmic Reticulum Stress
20. NF-Kappa B Signaling

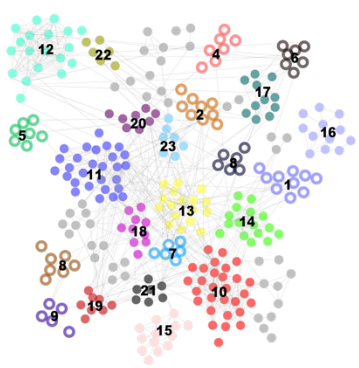

Clusters Upregulated in Response to mHTT in Neurons Only

1. TGF-Beta and Hippo Signaling Pathways
2. Cell Signaling/ Axon Guidance
3. Cellular Localization
4. Cell Division
5. Oligodendrocyte Differentiation
6. Vesicle Fusion and Exocytosis
7. Notch Signaling
8. Regulation of Secretions
9. Neuronal Ion Channel Clustering

Clusters Upregulated in Response to mHTT in Neurons or Glia

10. Extracellular Matrix Organization and Signaling
11. Receptor Mediated Cell Signaling
12. Endocytosis
13. Inflammation/Regulation of Transcription
14. Wound Healing and Inflammation
15. mRNA Processing
16. Endoplasmic Reticulum Stress
17. GTPase Signaling/ Actin Cytoskeleton
18. Cell Signaling
19. G-Protein Coupled Receptor Signaling
20. NF-Kappa B Signaling
21. Cell-Cell Adhesion
22. Fatty Acid Metabolism
23. Lipid Transport and Storage

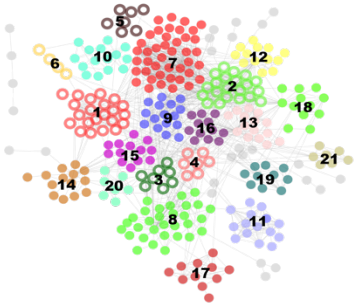

Clusters Downregulated in Response to mHTT in Glia Only

1. Synapse Assembly
2. Calcium Ion Transport
3. Regulation of Immune System and Metabolism
4. Phagocytosis
5. mRNA Processing
6. Fatty Acid Degradation

Clusters Downregulated in Response to mHTT in Neurons or Glia

7. Synaptic Transmission/ Cell Signaling
8. GTPase Signal Transduction
9. Synaptic Transmisssion/ Calcium Transport
10. Phospholipid Metabolism
11. Protein Ubiquitination
12. MAPK1 Signaling
13. Nervous System Development
14. Neurotransmitter Transport
15. Synaptic Reuptake
16. Axon Guidance and Development
17. GABAergic Synapse
18. Potassium Transport
19. Regulation of Potassium
20. Cytokine Singaling and Protein Transport
21. G2/M Cell Cycle Transition

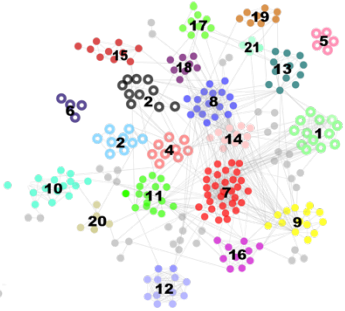

Clusters Downregulated in Response to mHTT in Neurons Only

1. Nucleotide Metabolism
2. Glycolysis
3. Cellular Respiration
4. Tricarboxylic Acid Cycle
5. Cell Adhesion
6. Glycosaminoglycan Synthesis

Clusters Downregulated in Response to mHTT in Neurons or Glia

7. Synaptic Transmission/ Cell Signaling
8. Synaptic Transmisssion/ Calcium Transport
9. MAPK1 Signaling
10. Phospholipid Metabolism
11. GTPase Signal Transduction
12. Protein Ubiquitination
13. Regulation of Potassium
14. Nervous System Development
15. GABAergic Synapse
16. Synaptic Reuptake
17. Potassium Transport
18. Axon Guidance and Development
19. Neurotransmitter Transport
20. G2/M Cell Cycle Transition
21. Cytokine Singaling and Protein Transport

Supplemental Figure 2. Network of DEGs responding concordantly to m*HTT* expression in glia or neurons, Related to Figure 2.

A) Heatmap representing all pairwise comparisons between clusters of upregulated (left) and downregulated (right) DEGs in response to glial (x-axis) or neuronal (y-axis) m*HTT* expression. Clusters are labeled using annotations for biological processes represented by DEGs within each cluster (Refer to **Tables S3**). Color is scaled to represent the significance of membership similarity calculated using a hypergeometric distribution. Colors represent the $-\log_{10}$(p-value) and range from white (5<) to dark red (>25).

B) PPI Network (STRING-db) of upregulated (top) and upregulated DEGs in human HD tissue, HD mouse models, and *Drosophila* expressing m*HTT* in glia.

C) PPI Network (STRING-db) of upregulated (top) and upregulated DEGs in human HD tissue, HD mouse models, and *Drosophila* expressing m*HTT* in neurons.

Refer to **Supplemental Table 3** for gene membership, as well as GO Panther and KEGG terms enriched genes within each cluster. Numbers in (B) and (C) correspond to annotations. Hollow circles correspond to clusters of DEGs that are dysregulated in response to m*HTT* (HTT^{FLQ200} or $HTT^{NT231Q128}$) expression in only glia (*repo-GAL4*) or neurons (*elav-GAL4*). Solid circles correspond to clusters of DEGs that are dysregulated in response to m*HTT* expression in neurons or glia.

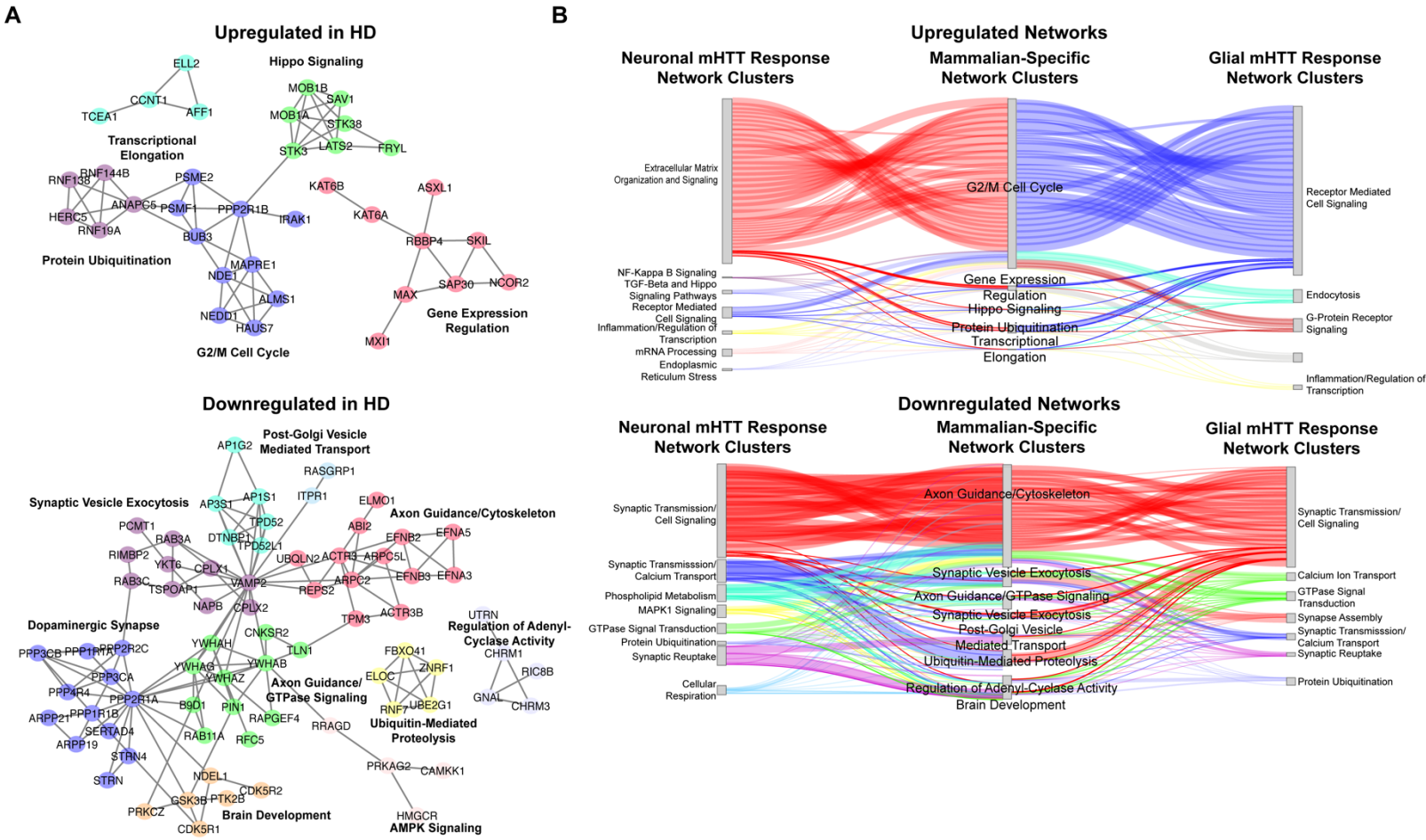

Supplemental Figure 3. Network of DEGs concordantly altered in human HD tissue and HD mouse models, but not in *Drosophila* HD models, Related to Figure 2.

A) Clustered, annotated PPI network (STRING-db) of DEGs concordantly upregulated (top) and downregulated (down) in human HD striatal tissue collected post-mortem (Hodges et al. 2006) and the allelic series of knock-in HD mouse models (Langfelder et al. 2016), but not in the *Drosophila* models (this study). Clusters are annotated for the synthesis of the top five most significantly enriched GO Panther Biological Process and KEGG terms (FDR<0.05).

B) Sankey plot for genes concordantly upregulated (top) and upregulated (bottom) in HD patients and mouse model only (middle) connecting to cluster of DEGs that are concordantly upregulated in patients, mice, and *Drosophila* as a consequence of expressing *mHTT* (HTT^{FLQ200} or $HTT^{NT231Q128}$) in neurons (*elav*) (left) or in glia (*repo*) (right). Edges represent protein-protein interactions between connected DEGs (STRING-db).

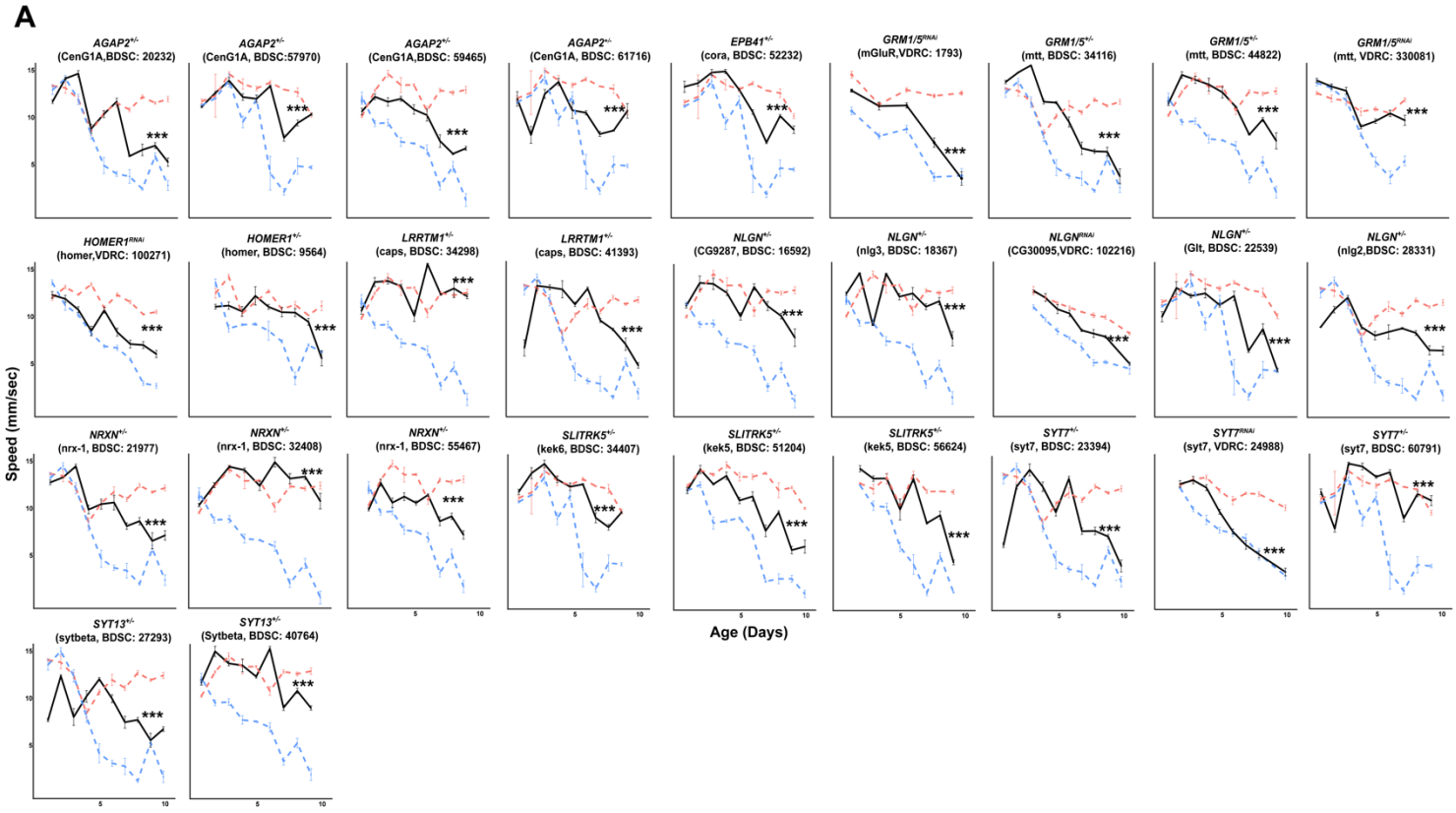

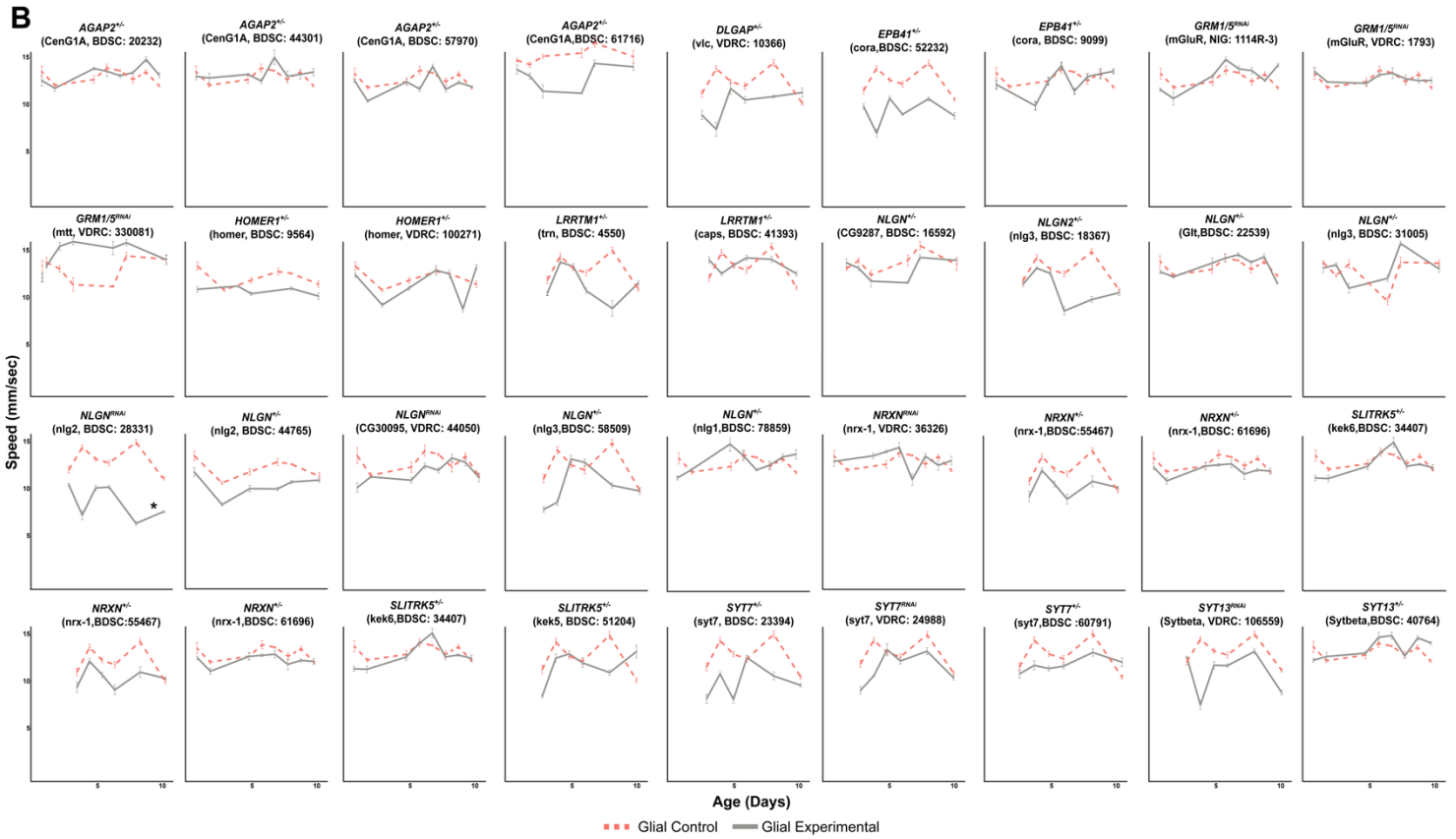

870

Supplemental Figure 4. Suppressors of glial mHTT-induced behavioral impairments among DEGs in the Synapse Assembly cluster, Related to Figure 3.

A) Representative graphs of behavioral assays (climbing speed as a function of time) of *Drosophila* expressing m*HTT* in glia (*repo>HTT*^{NT231Q128}) and alleles knocking down genes in the synapse assembly cluster. *** $p<0.001$ between the positive control (dashed blue line) and experimental allele (solid black line) by linear mixed effects model and post-hoc, pairwise analysis (see Methods). Refer to **Supplemental Table 4** for a summary of the full statistical analysis.

B) Representative graphs of the climbing speed of wildtype *Drosophila* as a function of time with the glial driver (*repo-GAL4*) expressing alleles that suppress glial mHTT-induced behavioral impairments. Points and error bars on the plot represent the mean speed ±SEM of three technical replicates. Each genotype was tested with 4-6 replicates of 10 animals. The gray line represents climbing speed of animals expressing the modifier allele in the *repo-GAL4* background.

Drosophila Genotypes: Positive control (*w*^{1118}*/+;UAS- non-targeting hpRNA/+; repo-GAL4,UAS-HTT*^{NT231Q128}*/+*), treatment control (*w*^{1118}*; repo-GAL4,UAS- HTT*^{NT231Q128}*/UAS-siHTT*), experimental (*w*^{1118}*; repo-GAL4,UAS- HTT*^{NT231Q128}*/modifier*), negative control (*w*^{1118}*; UAS- non-targeting hpRNA/+; repo-GAL4/+*), and experimental control (*w*^{1118}*; repo-GAL4/modifier*).

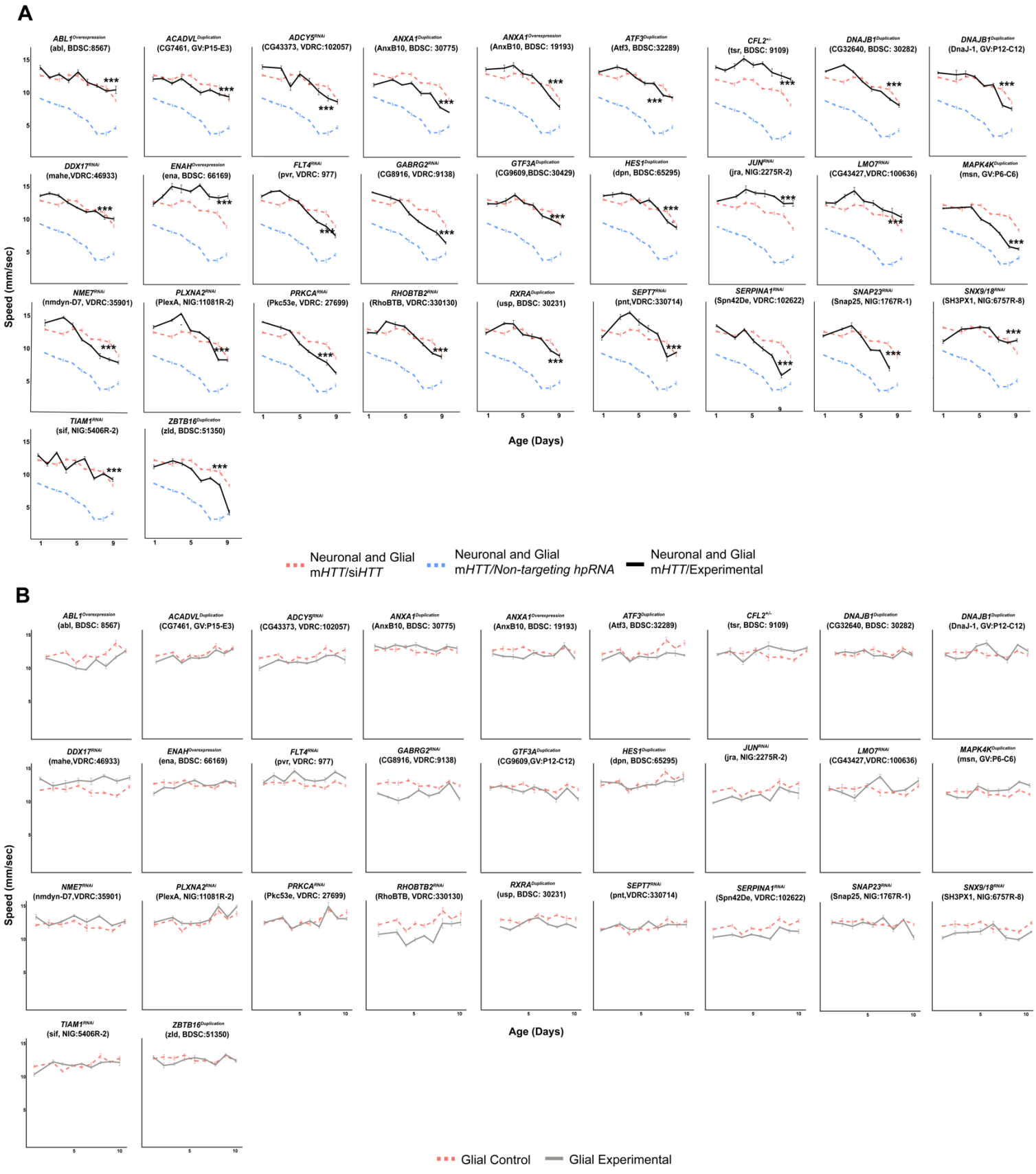

888

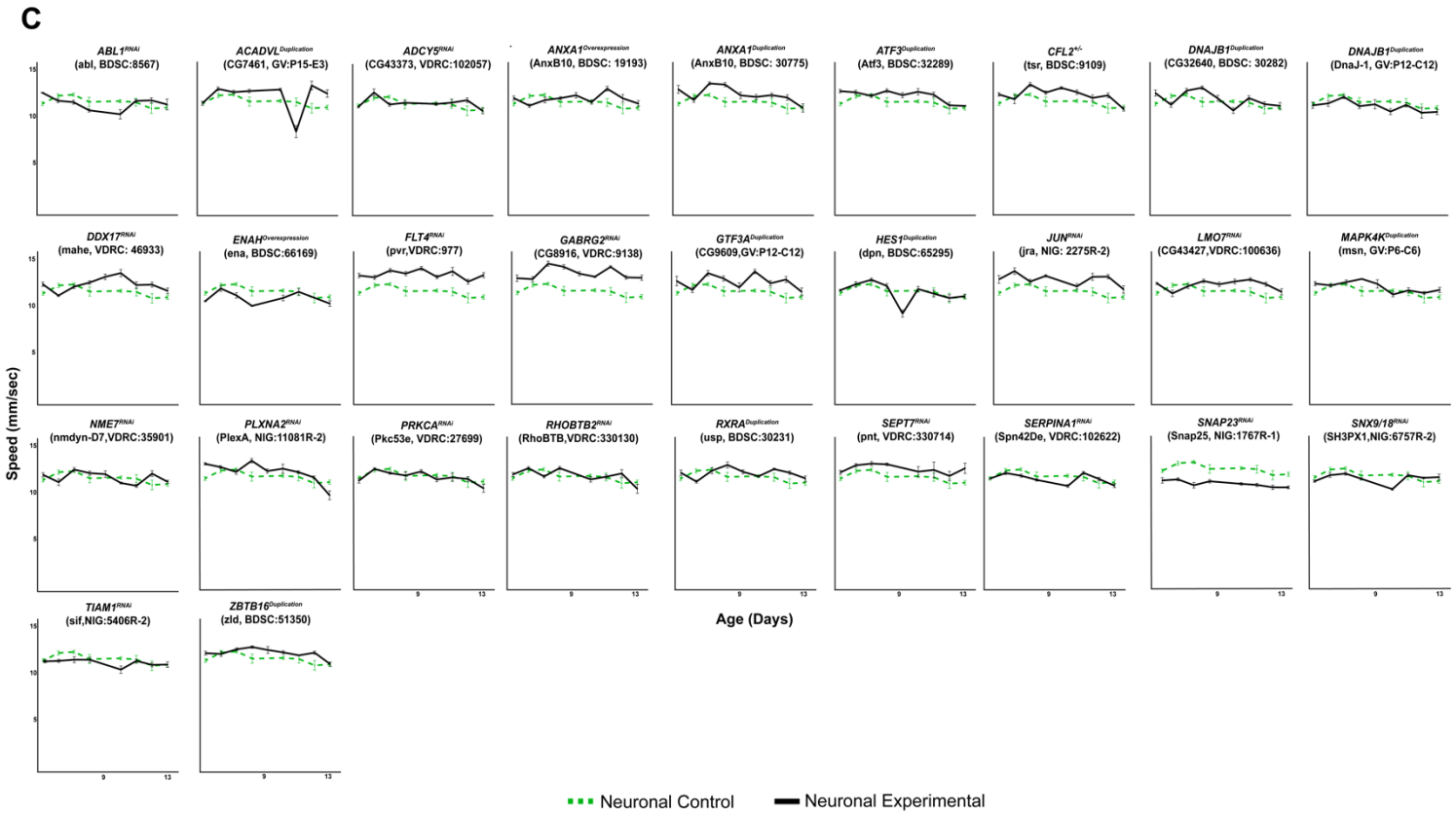

Supplemental Figure 5. Genetic modifiers suppress behavioral impairments caused by m*HTT* expression in neurons and glia, Related to Figure 5.

A) Representative graphs of the climbing speed of animals expressing mutant HTT in neurons and glia in combination with common modifiers as a function of time. *** $p<0.001$ between the positive control (dashed blue line) and experimental allele (solid black line) by linear mixed effects model and post-hoc, pairwise analysis. Refer to **Supplemental Table 6** for full statistical analysis of each genotype in neurons, glia, and both.

B) Representative graphs of the speed of wildtype *Drosophila* with the glial driver (*repo-GAL4)* and alleles that suppressed mutant HTT-induced behavioral impairments in both neurons and glia. The dashed red line represents the longitudinal climbing speed of animals expressing a non-targeting hpRNA in glia, while the gray line represents climbing speed of animals expressing the common modifier allele in the *repo-GAL4* background.

C) Representative graphs of the speed of wildtype *Drosophila* with the neuronal driver (*elav-GAL4)* expressing the alleles that suppressed mutant HTT-induced behavioral impairments in both neurons and glia as a function of time. The dashed green line represents the climbing speed of animals expressing a non-targeting hpRNA in neurons, while the black line represents climbing speed of animals expressing the common modifier allele in the *elav-GAL4* background.

Supplemental Figure 5 continued.

Points and error bars on the plot represent the mean speed ±SEM of three replicates. Each genotype was tested with 4-6 replicates of 10 animals.

Drosophila Genotypes: Neuronal and glial mHTT positive control (*elav^{c155}-GAL4/w^{1118};UAS-non-targeting hpRNA/+; repo-GAL4, UAS- HTT^{NT231Q128}*/+), neuronal and glial mHTT treatment control (*elav^{c155}-GAL4/w^{1118}; repo-GAL4, UAS-HTT^{NT231Q128}/UAS-siHTT*), neuronal and glial experimental (*elav^{c155}-GAL4/w^{1118}; repo-GAL4, UAS- HTT^{NT231Q128}/modifier*), glial control (*elav^{c155}-GAL4/w^{1118}; UAS-non-targeting hpRNA/+*), glial experimental control (*elav^{c155}-GAL4/w^{1118}; modifier/+*), neuronal control (*w^{1118}; UAS-non-targeting hpRNA/+; repo-GAL4/+*), and neuronal experimental control (*w^{1118}; repo-GAL4/modifier*).

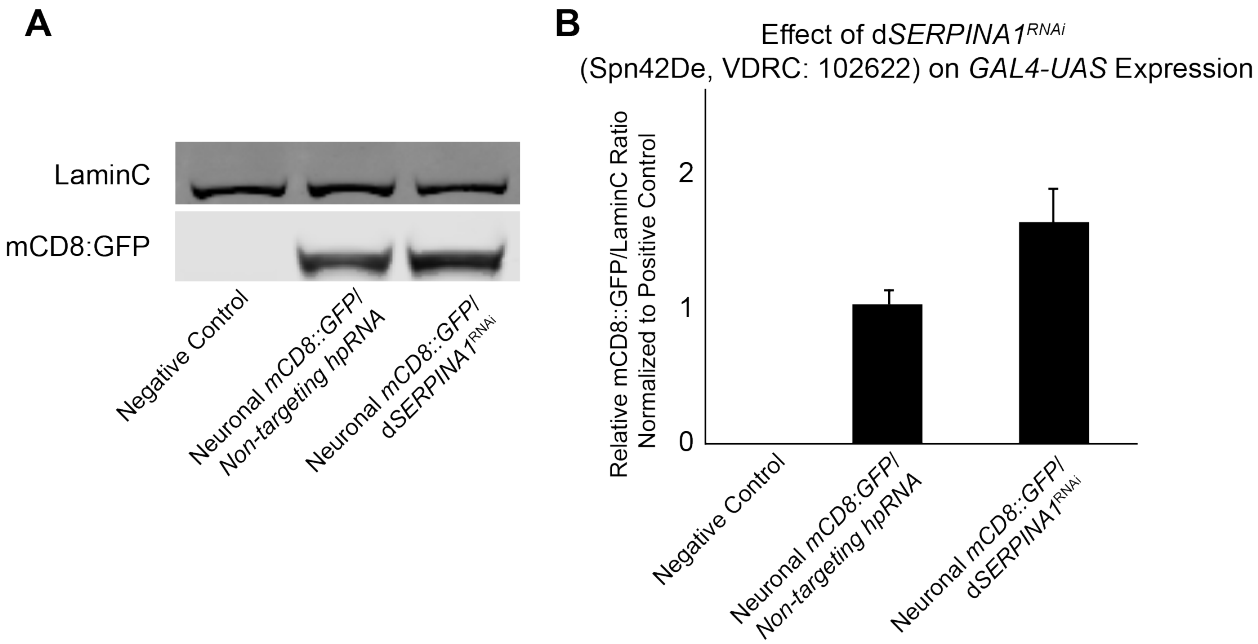

Supplemental Figure 6. d*SERPINA1* knockdown does not reduce the expression of the *GAL4-UAS* system, Related to Figure 6.

A) Representative immunoblot performed on *Drosophila* protein lysates assessing mCD8::GFP protein levels as a proxy for *GAL4-UAS* expression. *mCD8::GFP* was expressed in neurons using the *elav-GAL4* driver. The negative control in this experiment was *elav>GAL4* driving the expression of a non-targeting hpRNA (left lane). The positive control was *elav>GAL4* expressing the *mCD8::GFP* construct and a non-targeting hpRNA (middle lane). The experimental was *elav>GAL4* driving the expression of the *mCD8::GFP* construct and the d*SERPINA1*^{RNAi} (Spn42De, VDRC: 102622) allele that reduced mutant protein levels in **Figure 6** (right lane). LaminC was used as a loading control in this immunoblot.

B) Quantification of the three replicates from the immunoblot in (A) represented as the ratio of mCD8::GFP to LaminC, normalized to the average of the positive control.

930 **List of Supplemental Tables**

931

932 The following data sets (with the exception of Table S2 which can be found on page 33) are available at
933 http://bit.ly/Onur_et_al_supplement.

934

935 Table S1. Mappings of orthologous HD human, mouse, and *Drosophila* DEGs, Related to Figure 1.
936 Table S2. Network connectivity of DEGs responding to glial or neuronal m*HTT* expression, Related to
937 Figure 2.
938 Table S3. Cluster membership and summary of cluster annotations for DEGs responding to glial or
939 neuronal m*HTT* expression, Related to Figure 2.
940 Table S4. Summary of statistical analysis for alleles in the Synapse Assembly cluster that modify glial
941 mHTT-induced behavioral impairments, Related to Figure 3.
942 Table S5. Summary of alleles screened and results for common modifiers of mHTT-induced behavioral
943 impairments in neurons and glia, Related to Figure 5.
944 Table S6. Summary of statistics for alleles are common suppressors of neuronal and glial mHTT-induced
945 behavioral impairments, Related to Figure 5.

References

Abu-Rumeileh, S., Halbgebauer, S., Steinacker, P., Anderl-Straub, S., Polischi, B., Ludolph, A.C., Capellari, S., Parchi, P., and Otto, M. (2020). CSF SerpinA1 in Creutzfeldt-Jakob disease and frontotemporal lobar degeneration. Ann. Clin. Transl. Neurol. *7*, 191–199.

Al-Dalahmah, O., Sosunov, A.A., Shaik, A., Ofori, K., Liu, Y., Vonsattel, J.P., Adorjan, I., Menon, V., and Goldman, J.E. (2020). Single-nucleus RNA-seq identifies Huntington disease astrocyte states. Acta Neuropathol. Commun. *8*, 19.

Al-Ramahi, I., Lu, B., Di Paola, S., Pang, K., de Haro, M., Peluso, I., Gallego-Flores, T., Malik, N.T., Erikson, K., Bleiberg, B.A., et al. (2018). High-Throughput Functional Analysis Distinguishes Pathogenic, Nonpathogenic, and Compensatory Transcriptional Changes in Neurodegeneration. Cell Syst. *7*, 28-40.e4.

Barker, R.A., Fujimaki, M., Rogers, P., and Rubinsztein, D.C. (2020). Huntingtin-lowering strategies for Huntington's disease. Expert Opin. Investig. Drugs 1–8.

Barnat, M., Capizzi, M., Aparicio, E., Boluda, S., Wennagel, D., Kacher, R., Kassem, R., Lenoir, S., Agasse, F., Braz, B.Y., et al. (2020). Huntington's disease alters human neurodevelopment. Science *369*, 787–793.

Bayraktar, O.A., Bartels, T., Holmqvist, S., Kleshchevnikov, V., Martirosyan, A., Polioudakis, D., Ben Haim, L., Young, A.M.H., Batiuk, M.Y., Prakash, K., et al. (2020). Astrocyte layers in the mammalian cerebral cortex revealed by a single-cell in situ transcriptomic map. Nat. Neurosci. 500–509.

Benraiss, A., Wang, S., Herrlinger, S., Li, X., Chandler-Militello, D., Mauceri, J., Burm, H.B., Toner, M., Osipovitch, M., Jim Xu, Q., et al. (2016). Human glia can both induce and rescue aspects of disease phenotype in Huntington disease. Nat. Commun. *7*.

Blake, J.A., Eppig, J.T., Kadin, J.A., Richardson, J.E., Smith, C.L., Bult, C.J., and the Mouse Genome Database Group (2017). Mouse Genome Database (MGD)-2017: community knowledge resource for the laboratory mouse. Nucleic Acids Res. *45*, D723–D729.

Bondar, V.V., Adamski, C.J., Onur, T.S., Tan, Q., Wang, L., Diaz-Garcia, J., Park, J., Orr, H.T., Botas, J., and Zoghbi, H.Y. (2018). PAK1 regulates ATXN1 levels providing an opportunity to modify its toxicity in spinocerebellar ataxia type 1. Hum. Mol. Genet. *27*, 2863–2873.

Bradford, J., Shin, J.-Y., Roberts, M., Wang, C.-E., Li, X.-J., and Li, S. (2009). Expression of mutant huntingtin in mouse brain astrocytes causes age-dependent neurological symptoms. Proc. Natl. Acad. Sci. *106*, 22480–22485.

Buscemi, L., Ginet, V., Lopatar, J., Montana, V., Pucci, L., Spagnuolo, P., Zehnder, T., Grubišić, V., Truttman, A., Sala, C., et al. (2017). Homer1 Scaffold Proteins Govern Ca2+ Dynamics in Normal and Reactive Astrocytes. Cereb. Cortex *27*, 2365–2384.

Cabezas-Llobet, N., Camprubí, S., García, B., Alberch, J., and Xifró, X. (2018). Human alpha 1-antitrypsin protects neurons and glial cells against oxygen and glucose deprivation through inhibition of interleukins expression. Biochim. Biophys. Acta BBA - Gen. Subj. *1862*, 1852–1861.

983 Caron, N.S., Southwell, A.L., Brouwers, C.C., Cengio, L.D., Xie, Y., Black, H.F., Anderson, L.M., Ko,
984 S., Zhu, X., van Deventer, S.J., et al. (2020). Potent and sustained huntingtin lowering via AAV5
985 encoding miRNA preserves striatal volume and cognitive function in a humanized mouse model of
986 Huntington disease. Nucleic Acids Res. *48*, 36–54.

987 Chung, H., Wangler, M.F., Marcogliese, P.C., Jo, J., Ravenscroft, T.A., Zuo, Z., Duraine, L.,
988 Sadeghzadeh, S., Li-Kroeger, D., Schmidt, R.E., et al. (2020). Loss- or Gain-of-Function Mutations in
989 ACOX1 Cause Axonal Loss via Different Mechanisms. Neuron *106*, 589-606.e6.

990 Csardi, G., and Nepusz, T. The igraph software package for complex network research.

991 Darmanis, S., Sloan, S.A., Zhang, Y., Enge, M., Caneda, C., Shuer, L.M., Hayden Gephart, M.G., Barres,
992 B.A., and Quake, S.R. (2015). A survey of human brain transcriptome diversity at the single cell level.
993 Proc. Natl. Acad. Sci. *112*, 7285–7290.

994 Diaz-Castro, B., Gangwani, M.R., Yu, X., Coppola, G., and Khakh, B.S. (2019). Astrocyte molecular
995 signatures in Huntington's disease. Sci. Transl. Med. *11*.

996 Dietzl, G., Chen, D., Schnorrer, F., Su, K.-C., Barinova, Y., Fellner, M., Gasser, B., Kinsey, K., Oppel,
997 S., Scheiblauer, S., et al. (2007). A genome-wide transgenic RNAi library for conditional gene
998 inactivation in Drosophila. Nature *448*, 151–156.

999 Donnelly, K.M., DeLorenzo, O.R., Zaya, A.D., Pisano, G.E., Thu, W.M., Luo, L., Kopito, R.R., and
1000 Panning Pearce, M.M. (2020). Phagocytic glia are obligatory intermediates in transmission of mutant
1001 huntingtin aggregates across neuronal synapses. ELife *9*.

1002 Estrada Sánchez, A.M., Mejía-Toiber, J., and Massieu, L. (2008). Excitotoxic Neuronal Death and the
1003 Pathogenesis of Huntington's Disease. Arch. Med. Res. *39*, 265–276.

1004 Fernandez-Funez, P., Nino-Rosales, M.L., de Gouyon, B., She, W.C., Luchak, J.M., Martinez, P.,
1005 Turiegano, E., Benito, J., Capovilla, M., Skinner, P.J., et al. (2000). Identification of genes that modify
1006 ataxin-1-induced neurodegeneration. Nature *408*, 101–106.

1007 Ferrari Bardile, C., Garcia-Miralles, M., Caron, N.S., Rayan, N.A., Langley, S.R., Harmston, N.,
1008 Rondelli, A.M., Teo, R.T.Y., Waltl, S., Anderson, L.M., et al. (2019). Intrinsic mutant HTT-mediated
1009 defects in oligodendroglia cause myelination deficits and behavioral abnormalities in Huntington disease.
1010 Proc. Natl. Acad. Sci. *116*, 9622–9627.

1011 Filimonenko, M., Isakson, P., Finley, K.D., Anderson, M., Jeong, H., Melia, T.J., Bartlett, B.J., Myers,
1012 K.M., Birkeland, H.C.G., Lamark, T., et al. (2010). The selective macroautophagic degradation of
1013 aggregated proteins requires the PI3P-binding protein Alfy. Mol. Cell *38*, 265–279.

1014 Filipello, F., Morini, R., Corradini, I., Zerbi, V., Canzi, A., Michalski, B., Erreni, M., Markicevic, M.,
1015 Starvaggi-Cucuzza, C., Otero, K., et al. (2018). The Microglial Innate Immune Receptor TREM2 Is
1016 Required for Synapse Elimination and Normal Brain Connectivity. Immunity *48*, 979-991.e8.

1017 Freeman, M.R., and Doherty, J. (2006). Glial cell biology in Drosophila and vertebrates. Trends Neurosci.
1018 *29*, 82–90.

Garcia, V.J., Rushton, D.J., Tom, C.M., Allen, N.D., Kemp, P.J., Svendsen, C.N., and Mattis, V.B. (2019). Huntington's Disease Patient-Derived Astrocytes Display Electrophysiological Impairments and Reduced Neuronal Support. Front. Neurosci. *13*.

Gollin, P.A., Kalaria, R.N., Eikelenboom, P., Rozemuller, A., and Perry, G. (1992). Alpha 1-antitrypsin and alpha 1-antichymotrypsin are in the lesions of Alzheimer's disease. Neuroreport *3*, 201–203.

Goodman, L.D., Prudencio, M., Kramer, N.J., Martinez-Ramirez, L.F., Srinivasan, A.R., Lan, M., Parisi, M.J., Zhu, Y., Chew, J., Cook, C.N., et al. (2019). Toxic expanded GGGGCC repeat transcription is mediated by the PAF1 complex in C9orf72-associated FTD. Nat. Neurosci. *22*, 863–874.

Hodges, A., Strand, A.D., Aragaki, A.K., Kuhn, A., Sengstag, T., Hughes, G., Elliston, L.A., Hartog, C., Goldstein, D.R., Thu, D., et al. (2006). Regional and cellular gene expression changes in human Huntington's disease brain. Hum. Mol. Genet. *15*, 965–977.

Hong, Y., Zhao, T., Li, X.-J., and Li, S. (2016). Mutant Huntingtin Impairs BDNF Release from Astrocytes by Disrupting Conversion of Rab3a-GTP into Rab3a-GDP. J. Neurosci. *36*, 8790–8801.

Hu, Y., Flockhart, I., Vinayagam, A., Bergwitz, C., Berger, B., Perrimon, N., and Mohr, S.E. (2011). An integrative approach to ortholog prediction for disease-focused and other functional studies. BMC Bioinformatics *12*, 357.

Huang, B., Wei, W., Wang, G., Gaertig, M.A., Feng, Y., Wang, W., Li, X.-J., and Li, S. (2015). Mutant Huntingtin Downregulates Myelin Regulatory Factor-Mediated Myelin Gene Expression and Affects Mature Oligodendrocytes. Neuron *85*, 1212–1226.

Jiang, R., Diaz-Castro, B., Looger, L.L., and Khakh, B.S. (2016). Dysfunctional Calcium and Glutamate Signaling in Striatal Astrocytes from Huntington's Disease Model Mice. J. Neurosci. *36*, 3453–3470.

Kaltenbach, L.S., Romero, E., Becklin, R.R., Chettier, R., Bell, R., Phansalkar, A., Strand, A., Torcassi, C., Savage, J., Hurlburt, A., et al. (2007). Huntingtin Interacting Proteins Are Genetic Modifiers of Neurodegeneration. PLoS Genet. *3*, e82.

Kim, Y.J., Yi, Y., Sapp, E., Wang, Y., Cuiffo, B., Kegel, K.B., Qin, Z.-H., Aronin, N., and DiFiglia, M. (2001). Caspase 3-cleaved N-terminal fragments of wild-type and mutant huntingtin are present in normal and Huntington's disease brains, associate with membranes, and undergo calpain-dependent proteolysis. Proc. Natl. Acad. Sci. *98*, 12784–12789.

Langfelder, P., Cantle, J.P., Chatzopoulou, D., Wang, N., Gao, F., Al-Ramahi, I., Lu, X.-H., Ramos, E.M., El-Zein, K., Zhao, Y., et al. (2016). Integrated genomics and proteomics define huntingtin CAG length–dependent networks in mice. Nat. Neurosci. *19*, 623–633.

Langmead, B., and Salzberg, S.L. (2012). Fast gapped-read alignment with Bowtie 2. Nat. Methods *9*, 357–359.

Li, B., and Dewey, C.N. (2011). RSEM: accurate transcript quantification from RNA-Seq data with or without a reference genome. *12*.

Li, Z., Wang, C., Wang, Z., Zhu, C., Li, J., Sha, T., Ma, L., Gao, C., Yang, Y., Sun, Y., et al. (2019). Allele-selective lowering of mutant HTT protein by HTT–LC3 linker compounds. Nature *575*, 203–209.

1056 Lian, H., Yang, L., Cole, A., Sun, L., Chiang, A.C.-A., Fowler, S.W., Shim, D.J., Rodriguez-Rivera, J.,
1057 Taglialatela, G., Jankowsky, J.L., et al. (2015). NFκB-Activated Astroglial Release of Complement C3
1058 Compromises Neuronal Morphology and Function Associated with Alzheimer's Disease. Neuron *85*,
1059 101–115.

1060 Liddelow, S.A., Guttenplan, K.A., Clarke, L.E., Bennett, F.C., Bohlen, C.J., Schirmer, L., Bennett, M.L.,
1061 Münch, A.E., Chung, W.-S., Peterson, T.C., et al. (2017). Neurotoxic reactive astrocytes are induced by
1062 activated microglia. Nature *541*, 481–487.

1063 Litvinchuk, A., Wan, Y.-W., Swartzlander, D.B., Chen, F., Cole, A., Propson, N.E., Wang, Q., Zhang, B.,
1064 Liu, Z., and Zheng, H. (2018). Complement C3aR Inactivation Attenuates Tau Pathology and Reverses an
1065 Immune Network Deregulated in Tauopathy Models and Alzheimer's Disease. Neuron *100*, 1337-
1066 1353.e5.

1067 Love, M.I., Huber, W., and Anders, S. (2014). Moderated estimation of fold change and dispersion for
1068 RNA-seq data with DESeq2. Genome Biol. *15*.

1069 McInnes, J., Wierda, K., Snellinx, A., Bounti, L., Wang, Y.-C., Stancu, I.-C., Apóstolo, N., Gevaert, K.,
1070 Dewachter, I., Spires-Jones, T.L., et al. (2018). Synaptogyrin-3 Mediates Presynaptic Dysfunction
1071 Induced by Tau. Neuron *97*, 823-835.e8.

1072 McKinstry, S.U., Karadeniz, Y.B., Worthington, A.K., Hayrapetyan, V.Y., Ozlu, M.I., Serafin-Molina,
1073 K., Risher, W.C., Ustunkaya, T., Dragatsis, I., Zeitlin, S., et al. (2014). Huntingtin is required for normal
1074 excitatory synapse development in cortical and striatal circuits. J. Neurosci. Off. J. Soc. Neurosci. *34*,
1075 9455–9472.

1076 Miller, J.A., Menon, V., Goldy, J., Kaykas, A., Lee, C.-K., Smith, K.A., Shen, E.H., Phillips, J.W., Lein,
1077 E.S., and Hawrylycz, M.J. (2014). Improving reliability and absolute quantification of human brain
1078 microarray data by filtering and scaling probes using RNA-Seq. BMC Genomics *15*, 154.

1079 Nakanishi, M., Nomura, J., Ji, X., Tamada, K., Arai, T., Takahashi, E., Bućan, M., and Takumi, T.
1080 (2017). Functional significance of rare neuroligin 1 variants found in autism. PLOS Genet. *13*, e1006940.

1081 Neueder, A., Landles, C., Ghosh, R., Howland, D., Myers, R.H., Faull, R.L.M., Tabrizi, S.J., and Bates,
1082 G.P. (2017). The pathogenic exon 1 HTT protein is produced by incomplete splicing in Huntington's
1083 disease patients. Sci. Rep. *7*.

1084 Ochaba, J., Lukacsovich, T., Csikos, G., Zheng, S., Margulis, J., Salazar, L., Mao, K., Lau, A.L., Yeung,
1085 S.Y., Humbert, S., et al. (2014). Potential function for the Huntingtin protein as a scaffold for selective
1086 autophagy. Proc. Natl. Acad. Sci. *111*, 16889–16894.

1087 Octeau, J.C., Chai, H., Jiang, R., Bonanno, S.L., Martin, K.C., and Khakh, B.S. (2018). An Optical
1088 Neuron-Astrocyte Proximity Assay at Synaptic Distance Scales. Neuron *98*, 49-66.e9.

1089 Olsen, A.L., and Feany, M.B. (2019). Glial α-synuclein promotes neurodegeneration characterized by a
1090 distinct transcriptional program in vivo. Glia.

1091 O'Rourke, J.G., Gareau, J.R., Ochaba, J., Song, W., Raskó, T., Reverter, D., Lee, J., Monteys, A.M.,
1092 Pallos, J., Mee, L., et al. (2013). SUMO-2 and PIAS1 modulate insoluble mutant huntingtin protein
1093 accumulation. Cell Rep. *4*, 362–375.

1094 Osipovitch, M., Asenjo Martinez, A., Mariani, J.N., Cornwell, A., Dhaliwal, S., Zou, L., Chandler-
1095 Militello, D., Wang, S., Li, X., Benraiss, S.-J., et al. (2019). Human ESC-Derived Chimeric Mouse
1096 Models of Huntington's Disease Reveal Cell-Intrinsic Defects in Glial Progenitor Cell Differentiation.
1097 Cell Stem Cell *24*, 107-122.e7.

1098 Paris Autism Research International Sibpair Study, Jamain, S., Quach, H., Betancur, C., Råstam, M.,
1099 Colineaux, C., Gillberg, I.C., Soderstrom, H., Giros, B., Leboyer, M., et al. (2003). Mutations of the X-
1100 linked genes encoding neuroligins NLGN3 and NLGN4 are associated with autism. Nat. Genet. *34*, 27–
1101 29.

1102 Pearce, M.M.P., Spartz, E.J., Hong, W., Luo, L., and Kopito, R.R. (2015). Prion-like transmission of
1103 neuronal huntingtin aggregates to phagocytic glia in the Drosophila brain. Nat. Commun. *6*.

1104 Peng, S., Xu, J., Pelkey, K.A., Chandra, G., Zhang, Z., Bagh, M.B., Yuan, X., Wu, L.-G., McBain, C.J.,
1105 and Mukherjee, A.B. (2015). Suppression of agrin-22 production and synaptic dysfunction in *Cln1* $^{-/-}$
1106 mice. Ann. Clin. Transl. Neurol. *2*, 1085–1104.

1107 Phan, J.-A., Stokholm, K., Zareba-Paslawska, J., Jakobsen, S., Vang, K., Gjedde, A., Landau, A.M., and
1108 Romero-Ramos, M. (2017). Early synaptic dysfunction induced by α-synuclein in a rat model of
1109 Parkinson's disease. Sci. Rep. *7*.

1110 Prots, I., Grosch, J., Brazdis, R.-M., Simmnacher, K., Veber, V., Havlicek, S., Hannappel, C., Krach, F.,
1111 Krumbiegel, M., Schütz, O., et al. (2018). α-Synuclein oligomers induce early axonal dysfunction in
1112 human iPSC-based models of synucleinopathies. Proc. Natl. Acad. Sci. *115*, 7813–7818.

1113 Ring, K.L., An, M.C., Zhang, N., O'Brien, R.N., Ramos, E.M., Gao, F., Atwood, R., Bailus, B.J., Melov,
1114 S., Mooney, S.D., et al. (2015). Genomic Analysis Reveals Disruption of Striatal Neuronal Development
1115 and Therapeutic Targets in Human Huntington's Disease Neural Stem Cells. Stem Cell Rep. *5*, 1023–
1116 1038.

1117 Romero, E., Cha, G.-H., Verstreken, P., Ly, C.V., Hughes, R.E., Bellen, H.J., and Botas, J. (2008).
1118 Suppression of Neurodegeneration and Increased Neurotransmission Caused by Expanded Full-Length
1119 Huntingtin Accumulating in the Cytoplasm. Neuron *57*, 27–40.

1120 Rosvall, M., and Bergstrom, C.T. (2007). An information-theoretic framework for resolving community
1121 structure in complex networks. Proc. Natl. Acad. Sci. *104*, 7327–7331.

1122 Rosvall, M., and Bergstrom, C.T. (2008). Maps of random walks on complex networks reveal community
1123 structure. Proc. Natl. Acad. Sci. *105*, 1118–1123.

1124 Rousseaux, M.W.C., Vázquez-Vélez, G.E., Al-Ramahi, I., Jeong, H.-H., Bajić, A., Revelli, J.-P., Ye, H.,
1125 Phan, E.T., Deger, J.M., Perez, A.M., et al. (2018). A Druggable Genome Screen Identifies Modifiers of
1126 α-Synuclein Levels via a Tiered Cross-Species Validation Approach. J. Neurosci. *38*, 9286–9301.

1127 Sathasivam, K., Neueder, A., Gipson, T.A., Landles, C., Benjamin, A.C., Bondulich, M.K., Smith, D.L.,
1128 Faull, R.L.M., Roos, R.A.C., Howland, D., et al. (2013). Aberrant splicing of HTT generates the
1129 pathogenic exon 1 protein in Huntington disease. Proc. Natl. Acad. Sci. *110*, 2366–2370.

1130 Saudou, F., and Humbert, S. (2016). The Biology of Huntingtin. Neuron *89*, 910–926.

1131 Sofroniew, M.V. (2009). Molecular dissection of reactive astrogliosis and glial scar formation. Trends
1132 Neurosci. *32*, 638–647.

1133 Spampinato, S.F., Copani, A., Nicoletti, F., Sortino, M.A., and Caraci, F. (2018). Metabotropic Glutamate
1134 Receptors in Glial Cells: A New Potential Target for Neuroprotection? Front. Mol. Neurosci. *11*.

1135 Starz-Gaiano, M., Cho, N.K., Forbes, A., and Lehmann, R. (2001). Spatially restricted activity of a
1136 Drosophila lipid phosphatase guides migrating germ cells. Dev. Camb. Engl. *128*, 983–991.

1137 Stogsdill, J.A., Ramirez, J., Liu, D., Kim, Y.H., Baldwin, K.T., Enustun, E., Ejikeme, T., Ji, R.-R., and
1138 Eroglu, C. (2017). Astrocytic neuroligins control astrocyte morphogenesis and synaptogenesis. Nature
1139 *551*, 192–197.

1140 Südhof, T.C. (2008). Neuroligins and neurexins link synaptic function to cognitive disease. Nature *455*,
1141 903–911.

1142 Szklarczyk, D., Franceschini, A., Wyder, S., Forslund, K., Heller, D., Huerta-Cepas, J., Simonovic, M.,
1143 Roth, A., Santos, A., Tsafou, K.P., et al. (2015). STRING v10: protein–protein interaction networks,
1144 integrated over the tree of life. Nucleic Acids Res. *43*, D447–D452.

1145 Tabrizi, S.J., Leavitt, B.R., Landwehrmeyer, G.B., Wild, E.J., Saft, C., Barker, R.A., Blair, N.F.,
1146 Craufurd, D., Priller, J., Rickards, H., et al. (2019). Targeting Huntingtin Expression in Patients with
1147 Huntington's Disease. N. Engl. J. Med. *380*, 2307–2316.

1148 Tereshchenko, A.V., Schultz, J.L., Bruss, J.E., Magnotta, V.A., Epping, E.A., and Nopoulos, P.C. (2020).
1149 Abnormal development of cerebellar-striatal circuitry in Huntington disease. Neurology *94*, e1908–
1150 e1915.

1151 The Huntington's Disease Collaborative Research Group (1993). A novel gene containing a trinucleotide
1152 repeat that is expanded and unstable on Huntington's disease chromosomes. The Huntington's Disease
1153 Collaborative Research Group. Cell *72*, 971–983.

1154 Tong, X., Ao, Y., Faas, G.C., Nwaobi, S.E., Xu, J., Haustein, M.D., Anderson, M.A., Mody, I., Olsen,
1155 M.L., Sofroniew, M.V., et al. (2014). Astrocyte Kir4.1 ion channel deficits contribute to neuronal
1156 dysfunction in Huntington's disease model mice. Nat. Neurosci. *17*, 694–703.

1157 Trajkovic, K., Jeong, H., and Krainc, D. (2017). Mutant Huntingtin Is Secreted via a Late
1158 Endosomal/Lysosomal Unconventional Secretory Pathway. J. Neurosci. *37*, 9000–9012.

1159 Trotter, J.H., Dargaei, Z., Wöhr, M., Liakath-Ali, K., Raju, K., Essayan-Perez, S., Nabet, A., Liu, X., and
1160 Südhof, T.C. (2020). Astrocytic Neurexin-1 Orchestrates Functional Synapse Assembly (bioRxiv).

1161 Ushkaryov, Y., Petrenko, A., Geppert, M., and Sudhof, T. (1992). Neurexins: synaptic cell surface
1162 proteins related to the alpha-latrotoxin receptor and laminin. Science *257*, 50–56.

1163 Vaags, A.K., Lionel, A.C., Sato, D., Goodenberger, M., Stein, Q.P., Curran, S., Ogilvie, C., Ahn, J.W.,
1164 Drmic, I., Senman, L., et al. (2012). Rare Deletions at the Neurexin 3 Locus in Autism Spectrum
1165 Disorder. Am. J. Hum. Genet. *90*, 133–141.

1166 Vonsattel, J.P., Myers, R.H., Stevens, T.J., Ferrante, R.J., Bird, E.D., and Richardson, E.P. (1985).
1167 Neuropathological classification of Huntington's disease. J. Neuropathol. Exp. Neurol. *44*, 559–577.

1168 Wang, J., Gong, J., Li, L., Chen, Y., Liu, L., Gu, H., Luo, X., Hou, F., Zhang, J., and Song, R. (2018).
1169 Neurexin gene family variants as risk factors for autism spectrum disorder: Genetic risk for autism
1170 spectrum disorder. Autism Res. *11*, 37–43.

1171 Wang, N., Gray, M., Lu, X.-H., Cantle, J.P., Holley, S.M., Greiner, E., Gu, X., Shirasaki, D., Cepeda, C.,
1172 Li, Y., et al. (2014). Neuronal targets for reducing mutant huntingtin expression to ameliorate disease in a
1173 mouse model of Huntington's disease. Nat. Med. *20*, 536–541.

1174 Weiss, S., Melom, J.E., Ormerod, K.G., Zhang, Y.V., and Littleton, J.T. (2019). Glial Ca2+signaling links
1175 endocytosis to K+ buffering around neuronal somas to regulate excitability. ELife *8*.

1176 Wellington, C.L., Ellerby, L.M., Gutekunst, C.-A., Rogers, D., Warby, S., Graham, R.K., Loubser, O.,
1177 van Raamsdonk, J., Singaraja, R., Yang, Y.-Z., et al. (2002). Caspase cleavage of mutant huntingtin
1178 precedes neurodegeneration in Huntington's disease. J. Neurosci. Off. J. Soc. Neurosci. *22*, 7862–7872.

1179 Windrem, M.S., Osipovitch, M., Liu, Z., Bates, J., Chandler-Militello, D., Zou, L., Munir, J., Schanz, S.,
1180 McCoy, K., Miller, R.H., et al. (2017). Human iPSC Glial Mouse Chimeras Reveal Glial Contributions to
1181 Schizophrenia. Cell Stem Cell *21*, 195-208.e6.

1182 Wood, T.E., Barry, J., Yang, Z., Cepeda, C., Levine, M.S., and Gray, M. (2018). Mutant huntingtin
1183 reduction in astrocytes slows disease progression in the bachd conditional huntington's disease mouse
1184 model. Hum. Mol. Genet. *28*, 487–500.

1185 Yamamoto, A., Lucas, J.J., and Hen, R. (2000). Reversal of neuropathology and motor dysfunction in a
1186 conditional model of Huntington's disease. Cell *101*, 57–66.

1187 Yao, Y., Cui, X., Al-Ramahi, I., Sun, X., Li, B., Hou, J., Difiglia, M., Palacino, J., Wu, Z.-Y., Ma, L., et
1188 al. (2015). A striatal-enriched intronic GPCR modulates huntingtin levels and toxicity. ELife *4*.

1189 Yaylaoglu, M.B., Titmus, A., Visel, A., Alvarez-Bolado, G., Thaller, C., and Eichele, G. (2005).
1190 Comprehensive expression atlas of fibroblast growth factors and their receptors generated by a novel
1191 robotic in situ hybridization platform. Dev. Dyn. *234*, 371–386.

1192 Yuva-Aydemir, Y., Almeida, S., and Gao, F.-B. (2018). Insights into C9ORF72-Related ALS/FTD from
1193 Drosophila and iPSC Models. Trends Neurosci. *41*, 457–469.

1194 Zeng, X., Sun, M., Liu, L., Chen, F., Wei, L., and Xie, W. (2007). Neurexin-1 is required for synapse
1195 formation and larvae associative learning in *Drosophila*. FEBS Lett. *581*, 2509–2516.

1196 Ziegenfuss, J.S., Doherty, J., and Freeman, M.R. (2012). Distinct molecular pathways mediate glial
1197 activation and engulfment of axonal debris after axotomy. Nat. Neurosci. *15*, 979–987.

1198